NTNU

Norwegian University of
Science and Technology

High Arctic Sea-Ice Algae

The Use of Rapid Light Curves to Assess Photosynthetic Performance of Different Ice-Algal Communities

Marthe Sandbu

Marine Coastal Development
Submission date: February 2017
Supervisor: Geir Johnsen, IBI
Co-supervisor: Philipp Assmy, Norsk Polarinstitutt
Pedro Duarte, Norsk Polarinstitutt

Norwegian University of Science and Technology
Department of Biology

Abstract

The maximum quantum yield of charge separation in photosystem II ($\Phi PSII_{max}$) was assessed for studying the physiological performance of different ice algal communities and phytoplankton. By using rapid light curves (RLC), relative electron transfer rates (rETR) and photosynthetic parameters were calculated to determine whether photo-acclimation and light saturation (E_k) was evident for the algae sampled during early spring to early summer (March-June) at 80-83 °N off Spitsbergen. The highest photosynthetic responses, $\Phi PSII_{max}$ were found in thin ice and in pressure ridge communities in addition to the water column where a *Phaeocystis pouchetii* bloom took place in early June. This study indicates that in order to provide reliable estimates for the photosynthetic parameters (α_{rETR}, $rETR_{max}$ and E_k) using RLC, the samples need to reach light saturation plateau $rETR_{max}$, in order to understand the algae sample's ecological and physiological context. Challenges like low biomass of ice algae early in the sampling period provided rETR versus irradiance (E) curves that did not reach $rETR_{max}$. Modelling non-linear curves for these led to over-estimation of the saturation light parameter E_k. High photosynthetic performance with low signal-to-noise ratio and reliable rETR-E curves were however, made for the highly active algae within some communities. These communities are clear examples of how high Arctic ice-algae and phytoplankton exhibit acclimation traits to increasing irradiances and might lead to new eco-physiological hypotheses regarding the changing sea ice in the Arctic.

Sammendrag (Norsk)

Det maksimale kvanteutbyttet av ladningsseparasjon i fotosystem II ($\Phi PSII_{max}$) ble vurdert for å studere fysiologisk respons i ulike isalgesamfunn og for planteplankton. Ved å bruke «rapid light curves» (RLC), relativ elektron-overføringsrate (rETR) og fotosyntese-parametre ble beregnet til å vurdere foto-akklimatiseringsstatus og lysmetningsirradians (E_k) hos alger samlet fra tidlig vår til tidlig sommer (mars-juni) ved 80-83 °N for Spitsbergen. De høyeste responsene i $\Phi PSII_{max}$ ble funnet under tynn havis og i nedsenkede skrugarder, i tillegg til vannsøylen der en *Phaeocystis pouchetii* oppblomstring fant sted i begynnelsen av juni. Denne studien indikerer at for å fremkalle pålitelige estimater for fotosyntese-parametere (α_{rETR}, $rETR_{max}$ og E_k) ved hjelp RLC, må cellene nå lysmetningsplatået $rETR_{max}$, for å kunne forstå bedre sammenhengen mellom algenenes økologi og fysiologi. Utfordringer som lav biomasse av isalger tidlig i prøvetakningen, gav rETR versus irradians (E) -kurver som ikke nådde $rETR_{max}$. Modellerte ikke-lineære kurver for disse prøvene førte til overestimering av metningsirradiansparameteren E_k. Høy fotosyntetisk respons med lavt signal-til-støyforhold og pålitelige rETR-E-kurver ble imidlertid observert for noen av de aktive algesamfunnene. Disse samfunnene er derfor klare eksempler på hvordan arktiske isalger og planteplankton utfører foto-akklimatisering og tilpasning til økende irradianser, som kan føre til nye hypoteser rundt de økologiske endringene i havisen i Arktis.

Acknowledgement

First of all, I want to acknowledge the Norwegian Polar Institute (NPI) for the opportunity to join the N-ICE2015 project on such a short notice. I am thankful to have met and worked with the great researchers at NPI and my inspiring co-supervisors Philipp Assmy and Pedro Duarte. Your humbleness, knowledge and wisdom are truly appreciated and I will always have reverence for you. My sincere thanks to my supervisor at NTNU Prof. Geir Johnsen for his extreme passion for marine biology and his help regarding understanding the difficult field of photo-physiology and related mysteries of the oceans. Not only are you an inspiration for what a scientist should be like, but you are a great resource for your students at a personal level. I'm very grateful for the inspiration and interesting talks with the other researchers and colleagues I've met through NPI and Trondheim Biological Station (TBS) and those that have shared their data and knowledge with me. I want to thank my fellow master students at TBS who are supportive and passionate about marine biology and for being just awesome, young scientists – you are all inspiring to me! Late evenings with effective, and at times ineffective, work at TBS will be memories that will stick with me the rest of my life.

I would also like to acknowledge Dykkergruppa NTNUI for the amazing times we've had since I first arrived Trondheim as a student, five and a half years ago. Thank you for the opportunity to explore the underwater universe in a safe and fun way. I will forever be thankful to all of you and all the friendships I formed through our activities and at Dypet.

My dear family and friends: thank you for always being there for me when I need it. To mom, dad and my sisters; you are the foundation of my life and have showed me what's important in life. You let me follow my own path while supporting so – and now I have finally become a marine biologist, which I am proud to become. I would like to thank Runa for all support, great moments – big and small, or just that we "simply" got a dog together. Thanks to Marte Sofie for your fantastic support and wisdom. A phone-call away can really do wonders. And to my Audun, thank you for entering my life, I love you.

Table of Contents

Abbreviations

Symbol	Explanation	Unit
F_o	Minimum fluorescence in darkness	dimensionless
F_m'	Maximum fluorescence in actinic light	dimensionless
F_v'/F_m'	$(F_m'-F_o')/F_m'$: quantum yield of fluorescence in actinic light, Φ'PSII used for RLC	mol e^- · mol photons^{-1}
$\Phi PSII_{max}$	Maximum quantum yield of charge separation in photosystem II in dark-acclimated cells (30 min)	mol e^- · mol photons^{-1}
α_{rETR}	Maximum light utilization coefficient, initial slope of rETR versus irradiance curve	dimensionless
rETR	Relative electron transfer rate	dimensionless
	(Absolute ETR)	(mol e^- generated mol photons^{-1})
$rETR_{max}$	Maximum relative electron transfer rate	dimensionless
E_k	Irradiance (E) saturation parameter ($rETR_{max}/\alpha_{rETR}$), in older literature referred to as I_k	µmol photons · m^{-2} · s^{-1}
E_{PAR}	Irradiance (E) from the visible range of spectrum (Photosynthetic Active Radiation: 400-700 nm)	µmol photons · m^{-2} · s^{-1}
PAM	Pulse Amplitude Modulated fluorometer	
RLC	Rapid Light Curve	
P/E	Photosynthesis-irradiance, also referred to as P/I	
E&P	Eilers and Peeters (1988) equation	
J&P	Jassby and Platt (1976) equation	
Webb	Webb *et al.* (1974) equation	

Introduction

The Marine Arctic Sea Ice Ecosystem

Sea ice is one of the largest and extreme biomes on earth, but the interest of studying these ecosystems has only significantly been present for the last 40 years. Although sea ice microorganisms has a minor input to pan-Arctic primary production, due to the relative small volume of are they inhabit, the biomass concentrations in and on the underside of the ice can exceed those in seawater (Smetacek & Nicol, 2005). The sea ice micro-ecosystem is coupled to the pelagic or ice-associated (sympagic) fauna and the benthos as it contributes to sinking organic matter (Arrigo *et al*., 2014). Microorganisms such as bacteria, microalgae, micro-heterotrophs (heterotrophic flagellates and ciliates) and small crustaceans, experience strong gradients within the sea ice matrix with varying light and nutrient availability, low temperatures and extreme salinity ranges from 4-6 in annual ice to ~ 33-34 in Arctic Waters to > 60 PSU in brine (Arrigo & Thomas, 2004; Sakshaug *et al*. 2009).

Ice algae are ”upside-down” microphytobenthos that is being fed upon by sympagic fauna and provide, together with phytoplankton, the basis of the ice-associated marine ecosystems (Gradinger, 2009). The ice algal communities are generally dominated by pennate diatoms (class Bacillariophyceae), from the genera *Navicula*, *Nitzschia, Thalassiosira, Gyrosygma, Plaurosigma, Fragilariopsis, Fossula, Pinnularia* and the centric diatom *Melosira arctica.* They grow in different types of ice “habitats” like the interior layers of the sea ice, within brine channels and especially at the ice/water interface under the ice, known as bottom communities. The growth potential of ice algae differ from phytoplankton by their ability to grow and settle early in the season (starting in March and until summer melting season). Their extreme adaptation to low light and high brine salinities contributes to their success in the sea ice environment (McMinn & Hegseth, 2004). Phytoplankton in the high Arctic cannot bloom until late April, depending on latitude and lead formation - where light availability might increase rapidly and sustain a bloom for days or weeks. Some common genera for phytoplankton in the high Arctic are *Thalassiosira, Porosira, Chaetoceros* (centric diatoms) and the Prymnesiophyte *Phaeocystis pouchetii*.

Well-established ice algal communities are usually restricted to multi-year old sea ice (MYI) or thick first year ice (FYI), which is often dominated by the arborescent colony-forming diatom *Nitzschia frigida*. Where MYI is scarce, *e.g*. in the Barents Sea, the underside of the ice is typically covered by algae between early spring and ice melt. Little is known about the mechanisms for winter survival with a dark-period lasting up to 3 months, but some diatoms form resting spores or resting cells with gradually lowered metabolic rates, with high pigment content, carbohydrates or lipids. MYI is much more common for the Arctic than the Antarctic, due to the circulation patterns favouring for long-term ice growth. MYI differs from FYI by its longer life span, salinity gradient, and by containing much less brine and more air pockets. MYI is sea ice that has survived at least one summer melt with low salinities on top of the ice (at the snow-ice interface) that rises as a function of depth. FYI has salinity maximums at the top and the bottom of the ice. The life span of MYI can be < 7 years in the Arctic, but only up to 2 years in Antarctica. Most of the MYI in the Arctic Ocean is drifting pack ice in contrast to land-fast ice found in the frozen fjords of Svalbard, Greenland and northern Canada. (Syvertsen, 1991; Sakshaug *et al*., 2009; Thomas & Dieckmann, 2010)

As the thinning of sea ice continues together with the decline in its extent, due to the rapid warming of the Arctic ice cap, ice algal production of organic matter will likely be reduced in coming years and the sea ice ecosystem might be severely affected (Sakshaug *et al*., 2009; Arrigo *et al*., 2014). On the other side, light transmission will likely increase with thinner sea ice which can lead to massive phytoplankton blooms in nutrient-rich shelf waters in the Arctic (Arrigo *et al*., 2012). This leaves the question of whether primary production and carbon fixation will increase or decrease with the changes in the Arctic, open for further studies to investigate.

Irradiance, Chl *a* fluorescence & PAM fluorometry

Due to the extreme seasonal variation, irradiance (E, µmol photons m^{-2} s^{-1}) is inevitably one of the most important factors controlling primary production in Polar Regions (Smith & Sakshaug, 1990). Down-welling irradiance (E_d) varies from < 1 µmol photons m^{-2} s^{-1} to 1500 µmol photons m^{-2} s^{-1} from winter to summer (Manes & Gradinger, 2009). Day length, solar angle and cloudiness constitute the main components of the light climate and characterizing both spectral properties and amount of transmitted light through different media (snow, ice, and seawater) is crucial to determine the growth potential of an algal stock. Light intensity, or irradiance (E), can be measured in mol quanta or photons that hit a surface per unit of time (m^{-2} s^{-1}). E_{PAR} (µmol photons m^{-2} s^{-1}) is the irradiance measured within the photosynthetic active radiation, *i.e.* visible light spectrum: 400-700 nm. Furthermore, light emitted from cells (chlorophyll *a* fluorescence) can be used to measure certain qualities of a sample containing photosynthetic organisms, like the general physiological state/performance ($\Phi PSII_{max}$) under the generation of Rapid Light Curves (RLC), obtained with a Pulse Amplitude Modulation fluorometer (PAM).

The use of PAM fluorometry has become a common method to measure photosynthetic responses in plant leaves, and in macro- and microalgae (Sugett *et al*., 2010). The absorbed light energy has three competitive fates: photosynthesis (photochemistry), heat dissipation and re-emission of chlorophyll *a* (chl *a*) fluorescence (equation 1, Waltz, 2003; Maxwell & Johnson, 2000; Sugett *et al*., 2010). In living cells the fractions of photochemistry, heat dissipation and fluorescence is ~ 25-30 %, ~ 70 % and ~ 1-5 %, respectively (Roy *et al*., 2011). The principle of measuring variable chl *a* fluorescence is relatively simple and gives us information about electron transport and CO_2 assimilation rates in living organisms (Maxwell & Johnson, 2000; Baker & Oxborough, 2004). The red *in vivo* chl *a* fluorescence has two emission peaks at around 680 nm and 730 nm at room temperature (Johnsen & Sakshaug, 2007; Sakshaug *et al*. 2011; Sugett *et al*., 2010). Approximately 90-95 % of all the chl *a* fluorescence is emitted from photosystem II (PSII), which is measured by PAM. The amount of chl *a* bound to PSII versus photosystem I (PSI) differs between class/divisions of algae. For brown algae (class Phaeophyceae) ~ 80 % is bound to PSII. (Sakshaug et al., 2009; Sugett *et al*., 2010; Roy *et al*., 2011).

PAM's use of high intensity light results in multiple turnovers of the reactions centers (RC) in PSII (RCII), leading light energy to be emitted mainly as chl *a* fluorescence (Sugett *et al*., 2010). PSII is situated in the thylakoid membrane in the chloroplasts of algae. Applying a high-intensity saturation pulse (sat-pulse) causes saturating of all RCII and induces a fluorescence induction curve, which can provide information about the photosynthetic performance or the physiological state of a sample, *i.e*. the quantum yield of charge separation in PSII, $\Phi PSII_{max}$. The fluorescence induction curve reflects the electron transfer rate (photosynthesis) (Govindjee & Braun, 1974; Hancke *et al*., 2008). $\Phi PSII_{max}$ is simply the ratio of photons fluoresced to photons absorbed by PSII in dark-acclimated cells. The PAM instrument measures both minimum fluorescence from dark-acclimated samples and in actinic light (F_o and F_o') and the maximum fluorescence for both of these (F_m and F_m'), which produces the fluorescence induction curve, the $\Phi PSII_{max}$ and Φ'PSII (in actinic light, used to calculate electron transfer rates). $\Phi PSII_{max}$ needs to be calculated from dark acclimated cells because all (possible) RCII are open upon dark-acclimation. When the sat-pulse induces maximum fluorescence (F_m'), RCIIs close which provides the fluorescence yield, $\Phi PSII_{max.}$ (Genty *et al.,* 1989; Sugett *et al*., 2010). $\Phi PSII_{max}$ denotes the maximum fraction of open reaction centers of PSII (dark-acclimated cells, with maximum RCII that is oxidized/open), and thus reflect the cells ability to photosynthesize. The maximum theoretical value for $\Phi PSII_{max}$ is ~ 0.83 for <u>multiple turnover pulses</u> (like PAM), which means that 83 % of the RCII are open when the cells are dark-acclimated (Magnusson, 1997).

$$\underset{\sim 25\text{-}30\ \%}{\text{Photochemistry}} + \underset{\sim 1\text{-}5\ \%}{\text{fluorescence}} + \underset{\sim 70\ \%}{\text{heat}} = 1 \qquad (1)$$

Equation 1 shows how light energy captured by the light-harvesting antennae pigments in the thylakoid membrane, is converted into fractions of photochemistry, fluorescence and heat. Different types of light-harvesting pigments *e.g.* chlorophylls and carotenoids, capture photons, but the chl *a* molecule is always the last acceptor and is why we measure chl *a* fluorescence (Sugett *et al.*, 2010).

Fluorescence quenching

The fluorescence pathway can be affected in several ways, which challenges the use of chl *a* fluorescence to determine photosynthetic response. Photochemical quenching (PQ) *i.e*. photochemistry and non-photochemical quenching (NPQ), act to quench the fluorescence signal. NPQ includes several processes like heat dissipation, pH increase in the thylakoid lumen from intensified photosynthesis, and the amount of photo protective carotenoids (PPC). (Sugett *et al*., 2010). NPQ processes in particular, are important when interpreting for example PAM data.

Photo-adaptation and photo-acclimation

Many mechanisms are coinciding during photosynthesis, both long-term and short-term processes. Photo-acclimation is a physiological response to variation in the environment, often with regard to changes in irradiance and can occur from seconds (short-term) to days (long-term). At low irradiances algae need to maximize light harvesting capacity and photosynthetic efficiency. When irradiance becomes saturating, the Calvin cycle activity increases at the expense of light-harvesting pigments (Falkowski & LaRoche, 1991). At high irradiances a decline in pH inside the thylakoid lumen is normal due to the increased proton transport from the water splitting complex in PSII, which again leads to fluorescence quenching. The reduced pH can activate enzymes triggering short-term photo-acclimation such as the xanthophyll cycles that permits the excess of absorbed light energy to be released as heat (*i.e*. NPQ). Long-term photo-acclimation is mainly the change in composition and structure of the photosystems, *e.g.* changes in ratio between light-harvesting and photo-protective pigments or changes in chloroplast size and number. Photo-adaptation however, is the evolutionary change in gene expression due to the ongoing environmental changes. (Müller *et al*., 2001; Roy *et al*., 2011). Photo-adaptation may be important for ice algae and phytoplankton in the future Arctic Ocean due to more open waters and higher light transmission.

Rapid light curves to measure photo-physiological characteristics

A change in photosynthesis versus irradiance (P/E) curve parameters, such as the initial slope (α) and the light saturation parameter (E_k) can reflect acclimation to stress responses in the environment, and can be measured by steady-state light curves (LC) or rapid light curves (RLC), the latter having short light increments, usually < 30 seconds (Nitschke *et al*., 2012). RLC can provide valuable information regarding the overall photosynthetic performance of living cells, more specifically; the saturation characteristics of electron transport. Although traditional P/E curves and RLC have similar shapes with initial slope (α) and a saturating plateau, they are usually given in different units as well as describing similar, but different processes. The light increments for each irradiance level in a C_{14} P/E curve spans from minutes to hours, unlike for the RLC. C_{14} P/E curves estimates photosynthetic characteristics in either amount of carbon fixed or oxygen produced (oxygen evolution) per photons absorbed. (Ralph & Gademann, 2005)

Using RLC, the P/E curve is replaced by a rETR/E (or absolute ETR) curve to generate the photosynthetic parameters (α_{rETR}, $rETR_{max}$ and E_k). Despite the differences between P versus E and rETR versus E, the electron transfer rate (ETR) is closely related to the photosynthetic response, comparable to CO_2 uptake or oxygen evolution (Beer *et al*., 1998; Gilbert *et al*., 2000). Photo-acclimation processes might differ from each other since the cells have less time to recover under RLC than with longer increments (C_{14}), therefore the curves and parameters produced would likely differ. PAM is based on fluorescence and C_{14} on the uptake of a radioactive isotope. One would be careful to compare rETR/E and P/E curves for several reasons. The relative ETR may be calculated differently (depending on the author), but it describes well the relative changes in the photosynthetic rates (Sugett *et al*., 2010).

Usage of mathematical functions to reproduce photosynthetic light response

Mathematical formulation that produces the best fit between the equation and the experimental data is crucial for the interpretation of data gathered *in situ*. These equations provide photosynthetic parameters like α, P_{max} (maximum photosynthesis) and E_k, which exhibit valuable information regarding the physiology of photosynthetic algae (Jassby & Platt, 1976; Lederman & Tett, 1981; Eilers & Peeters, 1988). The choice of a suitable model requires information about the general physiology of the sample (*i.e.* species present and their light acclimation characteristics). For high Arctic sea-ice algae, such information is limited, since these communities have not been studied as intensively as phytoplankton. And this will lead to more challenging work regarding methods for measurements. (Waltz, 2003; Leu *et al*., 2015)

Aim

The purpose of this thesis is to study the method of using RLC to obtain information about the physiological condition of sea ice algae by using the maximum quantum yield of charge separation in photosystem II: $\Phi PSII_{max}$ and the light saturation parameter E_k as indicators. Furthermore, how this is linked to the physical conditions in the thinning Arctic ice sheet will be addressed for ecological context.

Materials and methods

Study area

The data for this master thesis were collected during the Norwegian young sea ICE (N-ICE2015) expedition led by the Norwegian Polar Institute (NPI). The expedition lasted from 15th of January to 26th of June 2015, drifting at ~ 80-83 °N in the thinner pack ice north of Svalbard (figure 1). The R/V Lance was frozen into the sea ice and anchored to follow the drift patterns and processes within, under and above the sea ice. Four different floes were in total surveyed for 111 days drifting with the ice, but the data used in this thesis was obtained from floe 2-4.

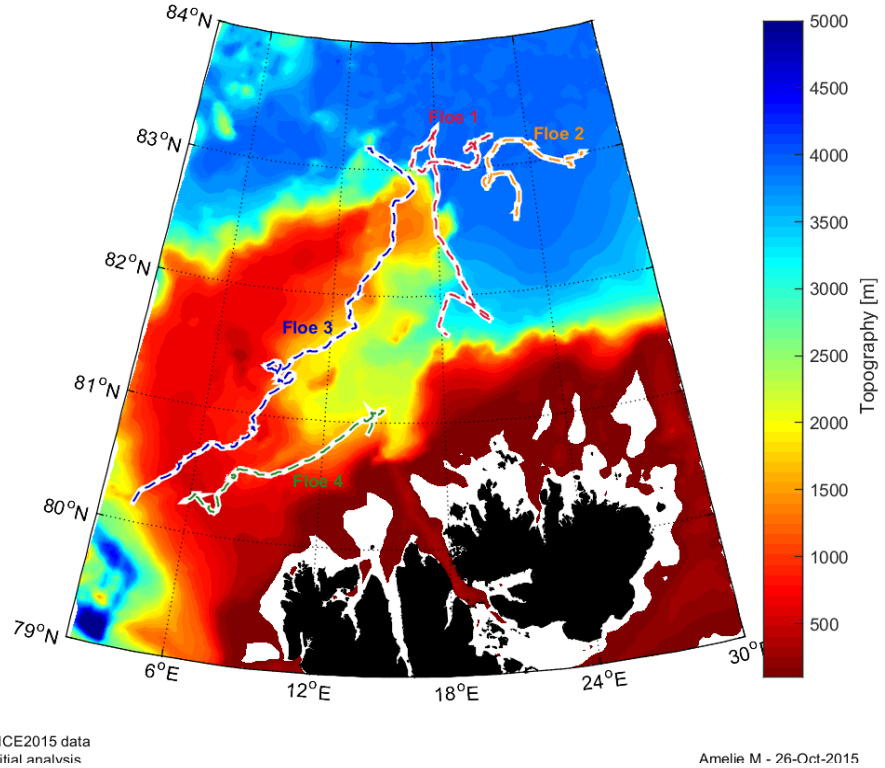

Figure 1: Drift trajectories of the four ice-floes monitored during N-ICE2015 superimposed on bottom topography. Floes 1 and 2 were drifted above the Arctic deep basin, while floes 3 and 4 mainly drifted over the Yermak plateau. (Map created by Amelie Meyer, NPI)

Snow and ice measurements

Snow and ice measurements were conducted by colleagues during the N-ICE2015 (Rösel *et al*., 2016a and b). Total snow and ice thickness were measured by an electromagnetic ground conductivity instument (EM31) that was dragged along ice transects manually while mounted to a sledge. Snow measurements were obtained by using a MagnaProbe (Snow-Hydro) equipped with a logger that recorded GPS coordinates simultaniously. Snow depths were subtracted from the total EM31 measurements to get ice thickness data. In addition ice and snow data in defines ice types; multi-year ice (MYI) and first year ice (FYI), obtained from drilling with auger flights (Kovacs Enterprise) and snow depth measured with a measuring tape .

Light measurements

Irradiance (E) data was conducted and processed by colleagues during the N-ICE2015 (Taskjelle *et al.,* 2016). Spectral irradiance (E_λ) was measured and intergrated in the PAR-region (400-700 nm) to provide E_{PAR}, with two RAMSES spectroradiometers (ACC-VIS, Trios GmbH, Germany) with planar cosine collectors that measured both incident and transmitted irradiance, on top and below the ice, respectively. These measurements were conducted at both floe 3 and 4 under thick snow-covered ice sites with a modal ice thickness of 1.46 ± 0.66 m and snow depth of 0.39 ± 0.21 m (Assmy *et al.,* 2017).

Phytoplankton/ice algae identification

Colleagues on the N-ICE2015 expedition did identification and counts of different taxa and species of algae samples (Assmy pers. Com.). Samples were settled in sedimentation chambers (HYRDO-BIOS©, Kiel, Germany) for 48 hours and thereafter counted at 100-600x magnifications with a Nikon Ti-S inverted light and epifluorescence microscope. In this thesis the dominant species/taxa for the peak days of $\Phi PSII_{max}$ (from different habitats) are the ones taken into consideration for simplifying the comparison with PAM data. The major taxa were mainly within the class of Bacillariophyceae (diatoms) in addition to some specific communities encountered during the expedition.

Chl *a* measurements

Chl *a* and phaeopigments (degraded chlorophyll pigments) samples were measured by a AU10 Turner Fluorometer (Turner Design, Inc.). 50-2000 ml (depending on biomass) of sample material was filtered through 25 mm GF/F Whatman filters. Filters were then put in light-protected chl *a* extraction tubes (10 ml) and 5 ml of 100 % methanol was added. Pigments were extracted in a refrigerator for approximately 12 hours. After extraction the tubes were mixed with a Vortex for a few seconds to get all pigment in suspension. Samples were transferred into a borosilicate cuvette, previously cleaned with 100 %. Chl *a* and phaeopigments were then measured in pigment extracts. First reading before acidification (Rb) was done which provided the Rb value and the total chlorophyll. Two drops of 5 % HCl were then added to the cuvette and blended carefully with parafilm on top to avoid spill. Then second reading by the fluorometer was carried out which provided the Ra (reading after acidification) value and the phaeopigment concentration. After acidification all chl *a* is degraded to phaeopigments and the difference between the two readings allows to calculate to concentration of chl *a* and that of phaeopigments separately. A methanol blank was put into the fluorometer to check that the cuvette was clean and that the fluorometer showed zero in pigment content. Pigment concentration (mg m^{-3}) was calculated according to a calibration following Knap *et al.* (1996).

Sampling of ice algae and phytoplankton

Sea ice samples obtained from ice coring were taken with a Kovacs Ice Corer with a diameter of 9 cm. Ice cores were covered by dark plastic bags to protect them from light before they were transported into a dark freezing container (- 20 °C). The bottom 10 cm of the cores (at the sea water-ice interface) were cut inside the freezer and placed into plastic buckets, protected from the light and with two parts of filtered seawater (FSW) to avoid osmotic shock during sea ice melting. Ice samples were melted in "room temperature" (~ 18-20 °C), for approximately 24 hours. Slush samples from snow-infiltration layers were not melted with FSW and therefore had less melting time and dilution than the ice samples. During the drift with ice-floe 3 water/slush samples from algal assemblages were collected by SCUBA-divers, using a "slurp gun" device (similar to a large-sized syringe) by gently sucking in seawater/slush and algae attached to the under-ice surfaces or those found at the top or on vertical walls of loose ice blocks along the ice ridges. Water samples with phytoplankton

were collected with Niskin bottles attached to a CTD. After melting of ice or directly sampled in the field, subsamples were taken out from their respective containers and put in a refrigerator to dark-acclimate for approximately 30 minutes before Pulse Amplitude Modulated (PAM) fluorometry analysis in the laboratory onboard the ship. These measurements were done keeping the samples in darkness inside the refrigerator under a temperature of 1-4 °C, close to *in situ* temperatures (Phyto-PAM optical fibers were passed through a hole in the refrigerator wall that was then closed with a plug to reduce air exchanges, figure 2a).

Phyto-PAM analysis

PAM fluorometry analysis of ice algae and phytoplankton was performed onboard the ship using a Phyto-PAM Phytoplankton Analyzer and the software Phyto-Win V 1.45 (Walz, Eiffeltrich, Germany). The instrument uses a high intensity LED (light emitting diode) -array as measuring light source with four different excitation wavelengths (table 1). The Phyto-ED (emitter-detector unit) was the measuring head that was used for measuring chl *a* fluorescence in algal samples (figure 2a). In this thesis only photosynthetic parameters obtained from the blue excitation channel (470 nm) were used in calculating the maximum quantum yield ($\Phi PSII_{max}$) and to produce estimates for rETR. This choice was made to optimize the signal-to-noise ratio (signal/noise) and due to the strong absorption by chl *c*, fucoxanthin and carotenoids in blue light by diatoms (Braun & Braun, 1974; Waltz, 2003; Johnsen & Sakshaug, 2007).

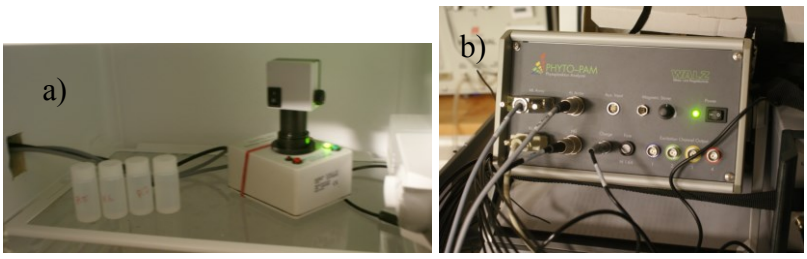

Figure 2: Stirring Device WATER-S, to keep cells in suspension inside the cuvette, mounted with the Emitter-Detector Unit PHYTO-ED and subsamples dark-acclimating inside the fridge **(a)** and the Power-and Control-Unit PHYTO-C **(b)**. (Images by M. S.)

Table 1: Fluorescence signal for different algal groups at the different excitation wavelengths, based on responses observed in pure cultures. (Waltz, 2003)

Excitation channel	Wavelength	Cyanobacteria	Green algae	Diatoms/dinoflagellates
1. Blue	470 nm	low	high	**high**
2. Green	520 nm		low	high
3. Red	645 nm	high		
4. Dark red	665 nm			

Settings for Phyto-PAM and RLC

The actinic light source was set to an irradiance of either 1 or 3 µmol photons m^{-2} s^{-1} for the first step of the rapid light curve and then increased up to 500-900 µmol photons m^{-2} s^{-1} (example in figure 3) using 20 second intervals (light increments) at each actinic light level. The saturation flash that induced the fluorescence induction curve was set to a duration time of 0.2 seconds (default setting), according to literature (Schreiber *et al*., 1995) with an intensity of 4000 µmol photons m^{-2} s^{-1} to rapidly close all reaction centers (all RCII reduced) and avoid photochemical quenching. $\Phi PSII_{max}$ values were obtained from first yield output, from dark-acclimated samples (equation 2, figure 3).

$$\Phi PSII_{max} = (F_m\text{-}F_o)/F_m \text{ (in dark-acclimated sample)} \quad (2)$$

$$\Phi'PSII = (F_m'\text{-}F_o')/F_m' \text{ (under actinic light)} \quad (3)$$

Unavoidable background fluorescence signal was digitally suppressed by using the automatic Zero-offset function (Zoff) in the software before running the RLC. In some samples background fluorescence signal was manually removed due to possible fluorescing particles besides the algal cells. A fluorescence blank was then obtained by filtering part of the sample with a 0.2 µm millipore filter, which was subtracted from the measured fluorescence induction curve values later (F1 and Fm1 in figure 3).

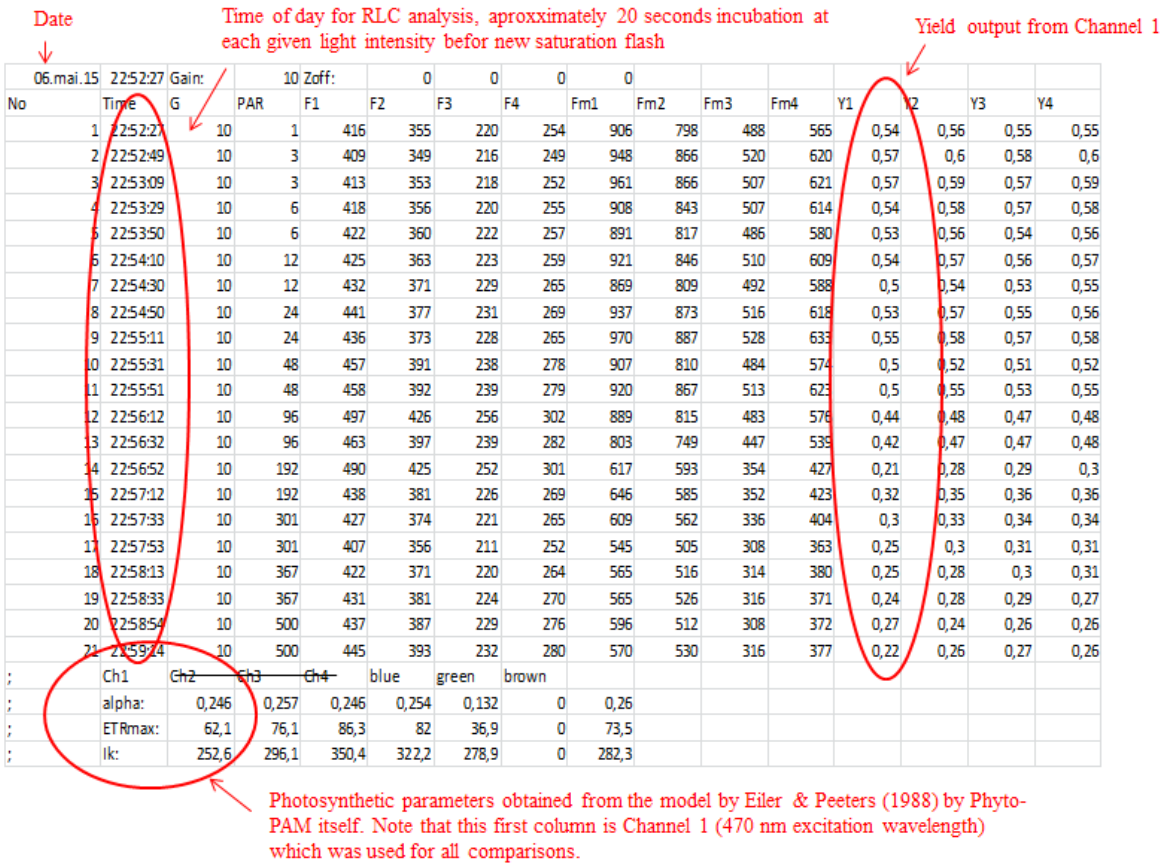

	06.mai.15	22:52:27	Gain:		10	Zoff:		0	0	0	0					
No		Time	G	PAR	F1	F2	F3	F4	Fm1	Fm2	Fm3	Fm4	Y1	Y2	Y3	Y4
	1	22:52:27	10	1	416	355	220	254	906	798	488	565	0,54	0,56	0,55	0,55
	2	22:52:49	10	3	409	349	216	249	948	866	520	620	0,57	0,6	0,58	0,6
	3	22:53:09	10	3	413	353	218	252	961	866	507	621	0,57	0,59	0,57	0,59
	4	22:53:29	10	6	418	356	220	255	908	843	507	614	0,54	0,58	0,57	0,58
	5	22:53:50	10	6	422	360	222	257	891	817	486	580	0,53	0,56	0,54	0,56
	6	22:54:10	10	12	425	363	223	259	921	846	510	609	0,54	0,57	0,56	0,57
	7	22:54:30	10	12	432	371	229	265	869	809	492	588	0,5	0,54	0,53	0,55
	8	22:54:50	10	24	441	377	231	269	937	873	516	618	0,53	0,57	0,55	0,56
	9	22:55:11	10	24	436	373	228	265	970	887	528	633	0,55	0,58	0,57	0,58
	10	22:55:31	10	48	457	391	238	278	907	810	484	574	0,5	0,52	0,51	0,52
	11	22:55:51	10	48	458	392	239	279	920	867	513	623	0,5	0,55	0,53	0,55
	12	22:56:12	10	96	497	426	256	302	889	815	483	578	0,44	0,48	0,47	0,48
	13	22:56:32	10	96	463	397	239	282	803	749	447	539	0,42	0,47	0,47	0,48
	14	22:56:52	10	192	490	425	252	301	617	593	354	427	0,21	0,28	0,29	0,3
	15	22:57:12	10	192	438	381	226	269	646	585	352	423	0,32	0,35	0,36	0,36
	16	22:57:33	10	301	427	374	221	265	609	562	336	404	0,3	0,33	0,34	0,34
	17	22:57:53	10	301	407	356	211	252	545	505	308	363	0,25	0,3	0,31	0,31
	18	22:58:13	10	367	422	371	220	264	565	516	314	380	0,25	0,28	0,3	0,31
	19	22:58:33	10	367	431	381	224	270	565	526	316	371	0,24	0,28	0,29	0,27
	20	22:58:54	10	500	437	387	229	276	596	512	308	372	0,27	0,24	0,26	0,26
	21	22:59:14	10	500	445	393	232	280	570	530	316	377	0,22	0,26	0,27	0,26
;		Ch1	~~Ch2~~	~~Ch3~~	~~Ch4~~	blue	green	brown								
;		alpha:	0,246	0,257	0,246	0,254	0,132	0	0,26							
;		ETRmax:	62,1	76,1	86,3	82	36,9	0	73,5							
;		Ik:	252,6	296,1	350,4	322,2	278,9	0	282,3							

Figure 3: Example of the Phyto-PAM output when constructing a RLC with 20 seconds time steps between each actinic light level E_{PAR} ("PAR"), F_o and F_o' (F1 column) and F_m and F_m' (Fm1 column) for channel 1 (470 nm) and the corresponding yields $\Phi PSII_{max}$/Φ'PSII (Y1 column). The $\Phi PSII_{max}$ is 0.54 for the dark-acclimated sample. The calculated photosynthetic parameters (α_{rETR}, $rETR_{max}$ and E_k) estimated with the Eilers and Peeters (1988) non-linear model (by the Phyto-PAM software) are 0.246, 62.1 and 252.6 respectively.

Data analysis and processing of PAM data

The report files from the software (figure 3) were later imported into an Excel worksheet for $\Phi PSII_{max}$ and Φ'PSII corrections and rETR calculations. Outliers were removed, *i.e.* ΦPSII values that was not in the 0-0.83 range. Relative electron transfer rates (rETR) were calculated according to the Waltz (2003) manual:

$$rETR = \Phi_{PSII} \cdot E_{PAR} \cdot 0.84 \cdot 0.5, \quad (4)$$

where 0.84 is the absorptivity of higher plant leaves (here used for phytoplankton for comparable results) and 0.5 (50 % of the light energy) is the assumed fraction of incident E_{PAR} that is absorbed and utilized by PSII (Waltz, 2003). PAM does not measure the effective absorption cross section of PSII that is necessary to estimate absolute ETR (µmol electrons m^{-2} s^{-1}). (Removing the two constants 0.84 and 0.5 gave minor change in the rETR data points.)

Irradiance calibration and check of E_{PAR} in Phyto-PAM software

To ensure a that RLC has true irradiance levels, a test with two differently calibrated scalar E_{PAR} sensors (US-SQS/L Spherical Micro Quantum Sensor, Effeltrich, Germany) was made to validate the irradiance output of the Phyto-PAM. An amplifier (US-SQS/B-D, Effeltrich, Germany) was connected to the light-sensors and were put inside the cuvette filled with distilled water in the ED unit. The instrument output was quite comparable to the E_{PAR} of the two light-sensors (figure 4).

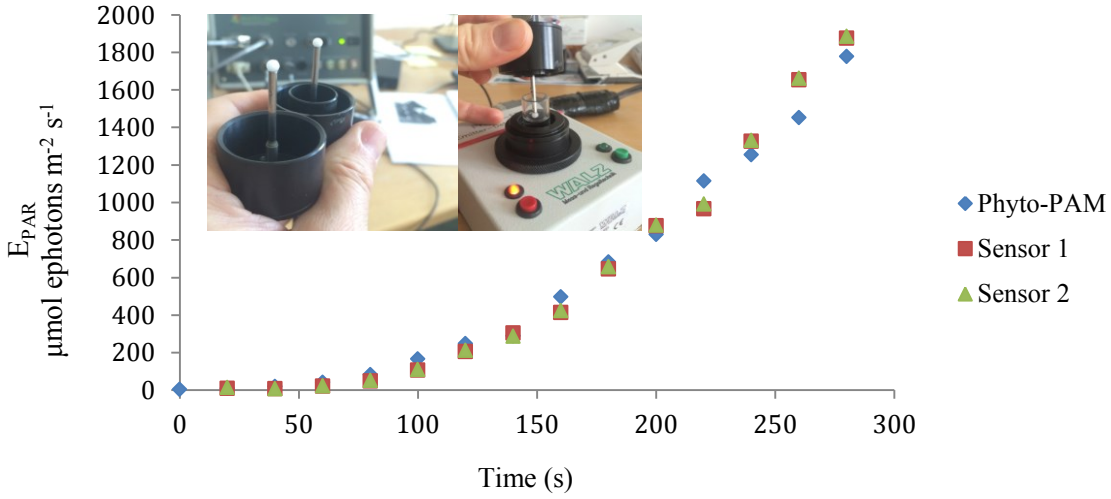

Figure 4: Light validation on E_{PAR} from Phyto-PAM and the two irradiance sensors (tested at the Fram Centre, Tromsø, February 2016). Images by M. S.

Fitting rETR versus E data with different equations for obtainment of photosynthetic parameters

Non-linear curve regressions were done for all samples with reliable $\Phi PSII_{max}$ values in KalaidaGraph 4.5 (demo). This was to produce α, $rETR_{max}$, and E_k estimates and to study the shape of the modelled curve. Since the Phyto-PAM software produced the Eilers and Peeters (1988) estimates, two additional models were used with the curve fitting procedure:

Eilers and Peeters (1988): $ETR = \frac{E_{PAR}}{\alpha \cdot E_{PAR} + b \cdot E_{PAR} + c}$ (5)

Jassby and Platt (1976): $ETR = rETRmax \cdot TanH(\alpha_{rETR} \cdot E_{PAR}/rETR_{max})$ (6)

Webb *et al.* (1974): $ETR = rETR_{max}(1-\exp(-\alpha_{rETR} \cdot E/ rETR_{max}))$ (7)

Results

The environmental data was collected, analyzed and graphically prepared by colleagues (with some modifications) working on the N-ICE2015 project. This section is used to elaborate the environmental conditions that were present during the expedition.

Snow and ice thickness distribution

Snow and ice thickness distribution on all ice-floes showed mainly a dominance of first year ice (FYI) and second year ice (SYI), in addition to some multi-year ice (MYI). The mean snow thickness distribution was relatively similar between the different ice-floes with a mean ~ 50 cm on ice-floe 2-3 and ~ 20 cm one ice-floe 4. The ice thickness distribution also exhibited similarity between the floes with a mean thickness ~ 1 m. A slightly higher fraction of thick MYI (2-4 m) was present on ice-floe 2 and 3.

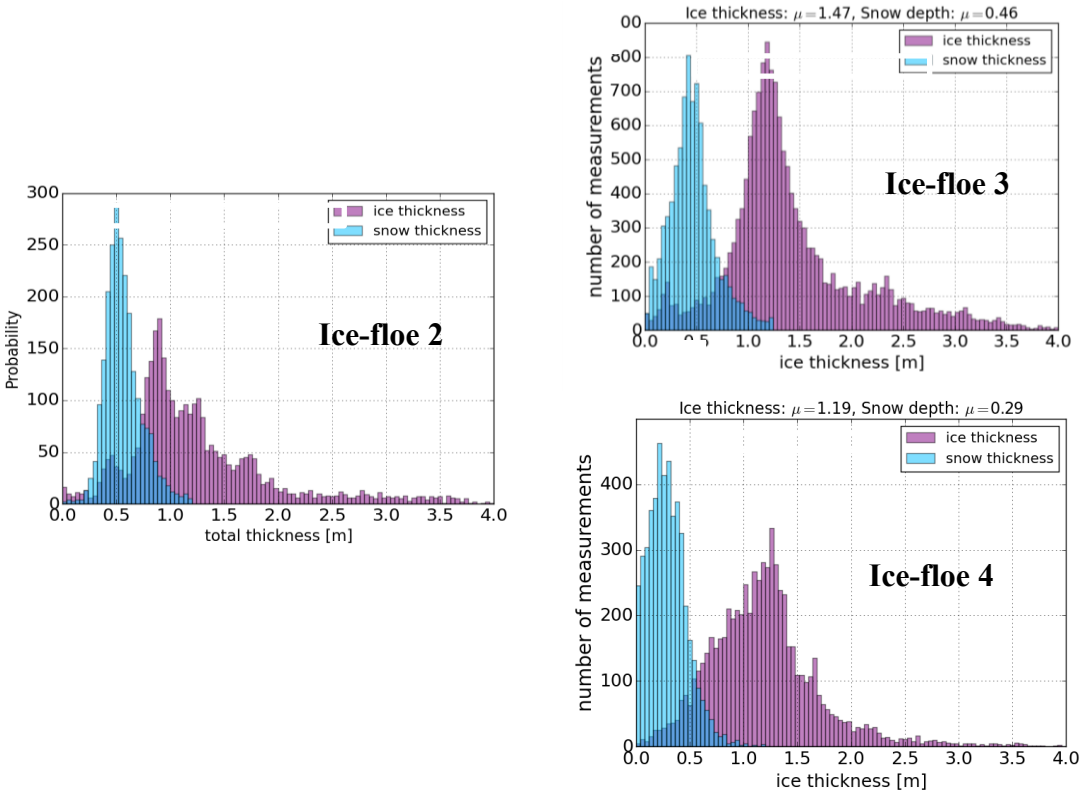

Figure 5: Ice and snow thickness distribution on ice-floes 2-4. Measurements were obtained with an EM31 (total ice and snow) and MagnaProbe (snow). (Graphics from Rösel A.)

Table 2: Ice and snow data obtained from drilling in defines ice types; second-year ice (SYI)/multi-year ice (MYI) and first year ice (FYI) from March to June. (Data from Rösel *et al*., 2016)

Ice station	Ice thickness (cm)	Snow depth (cm)	Freeboard (cm)	Ice type	Date
Floe 2	98	25	2	FYI	05.03.15
	70	35	-3	FYI	12.03.15
	125	45	-3	FYI	18.03.15
Floe 3	138	47	1	MYI	30.04.15
	143	46	1	MYI	07.05.15
	138	NA	2	MYI	14.05.15
	132	42	1	MYI	21.05.15
	126	41	0	MYI	28.05.15
	122	NA	0	MYI	04.06.15
Floe 4	109	28	-2	MYI	13.06.15
(ice floe was very patchy FYI/MYI)	88	7 cm snow+ 10cm ice crust	-6	FYI	17.06.15

Under-ice irradiance

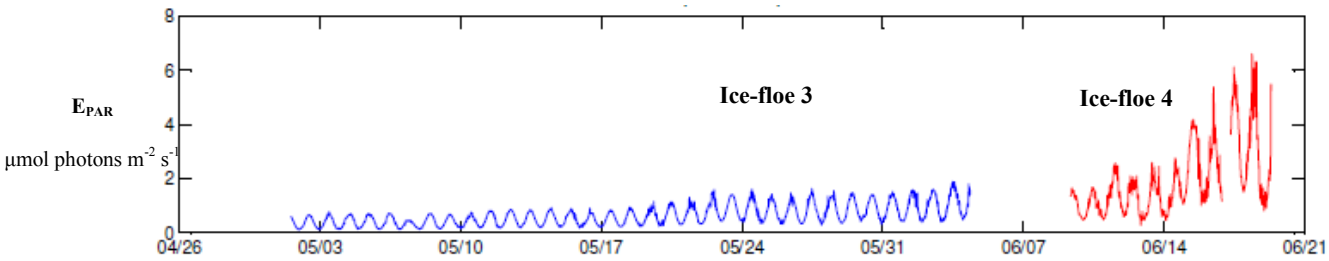

Figure 6: Transmitted E_{PAR} from under thick ice measured with two RAMSES spectro-radiometers (sum 400-700 nm). Ice thickness on the RAMSES setup site on ice-floe 3 and 4 was 130 cm and 120 cm, respectively. Snow depth however, was 40 cm on floe 3 and 15-20 cm on floe 4. Diurnal changes are indicated by highs and lows and increased in amplitude later in the season. (Data and graphics from Taskjelle *et al*, 2016)

Ice algae and phytoplankton observations

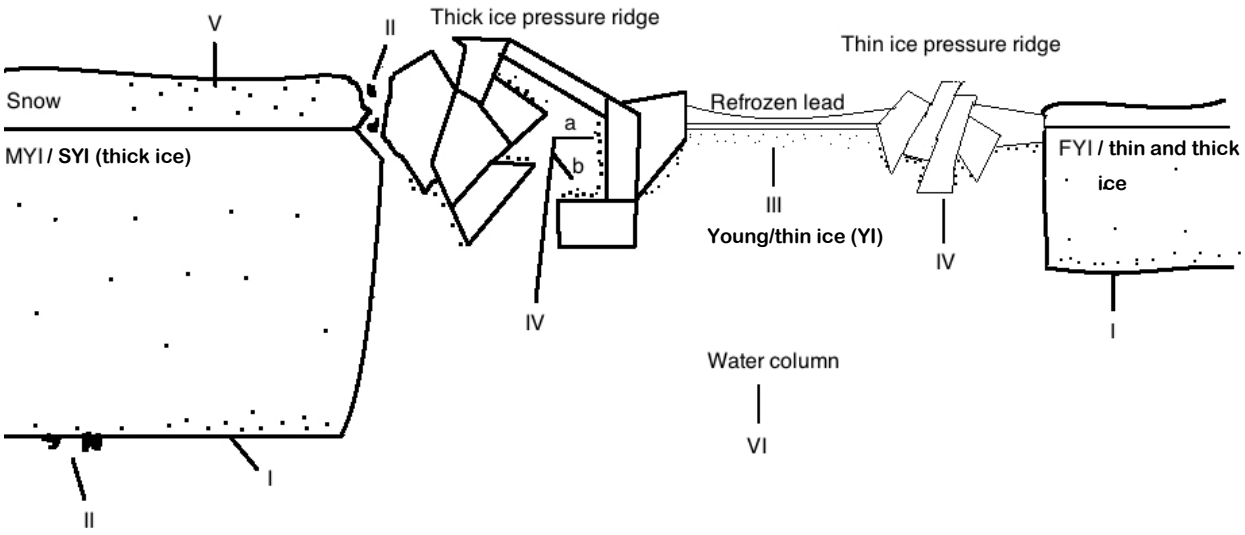

Figure 7: Observed algal communities during the N-ICE2015 expedition on ice-floe 2-3 merged into one illustration. I: bottom communities, II: ice-algal aggregates (bleached lumps and partly living cells) frozen on the underside of the ice, III: newly colonized refrozen leads where a high density of the photosynthetic ciliate *Mesodinium rubrum* was observed in early May, IV: pressure ridge communities with dominance of *Nitschia frigida* in vertical ledges (a) and *Thalassiosira bioculata* in horizontal (b) ones (mid-May), V: snow infiltration community dominated by diatoms and the planktonic Prymnesiophyte *Phaeocystis pouchetii* observed on ice-floe 4 and VI: water column where a *P. pouchetii* bloom occurred in June (Assmy *et al*. 2017). Note that this is a rough sketch on where the different active algal assemblages/communities were found throughout the whole expedition. Illustration M. S.

Figure 8: The autotrophic ciliate *Mesodinium rubrum* (15-70 µm) captured under the light microscope. (Image: Assmy P.)

Temporal ΦPSII$_{max}$ and sampling types

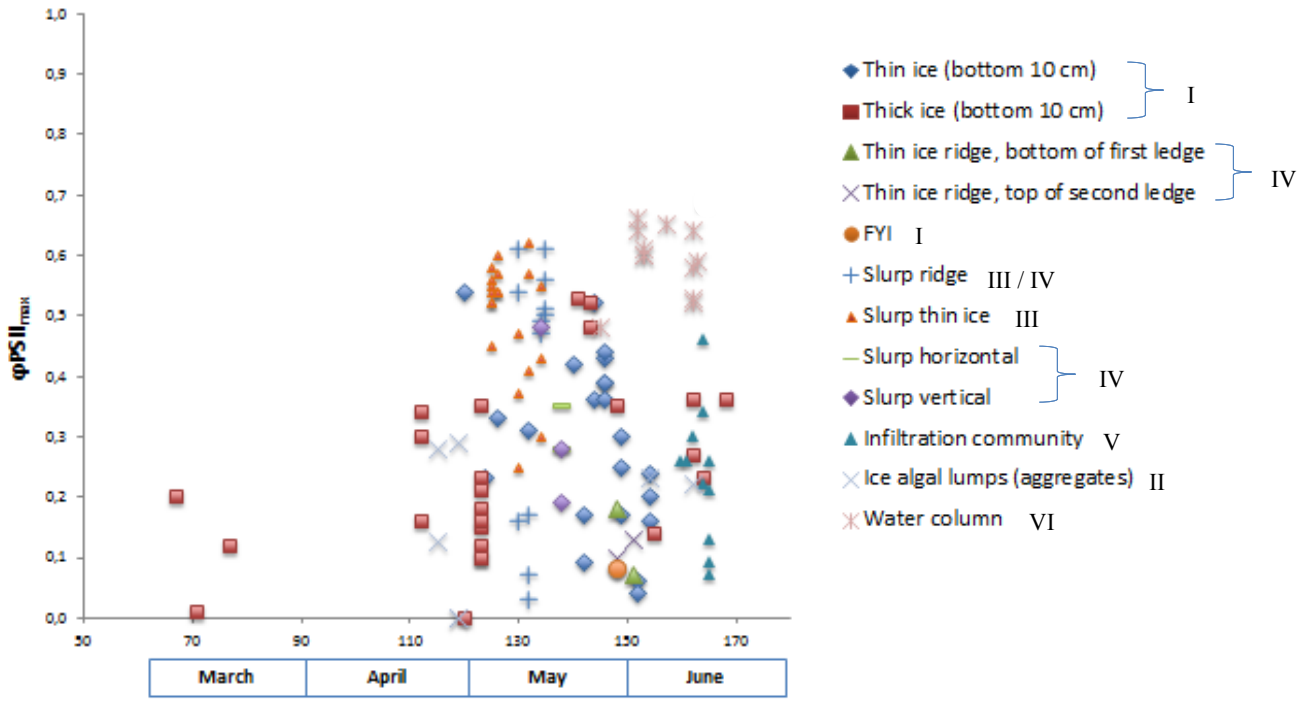

Figure 9: ΦPSII$_{max}$ in different habitats, obtained with various sampling methods plotted against day of the year. The habitat numbers from figure 8 is incorporated into the side legend. Red squares: thick second-year ice (SYI) merged with multi-year old ice (MYI) that was sampled throughout the whole expedition, showed a significant increase in ΦPSII$_{max}$ from early March to late June. Purple crosses: water column showed the highest responses in total (ΦPSII$_{max}$ = 0.66), with the *Phaeocystis pouchetii* bloom in early June (Assmy *et al*., 2017). The "slurp" samples are water/slush with algae from under thin ice and ridges obtained with SCUBA. These values were relatively high with ΦPSII$_{max}$ ~ 0.6. There is much variation within some habitats such as thin and thick ice and the snow infiltration layer. The gap between measurements is due to the crew shift in end of March to mid-April.

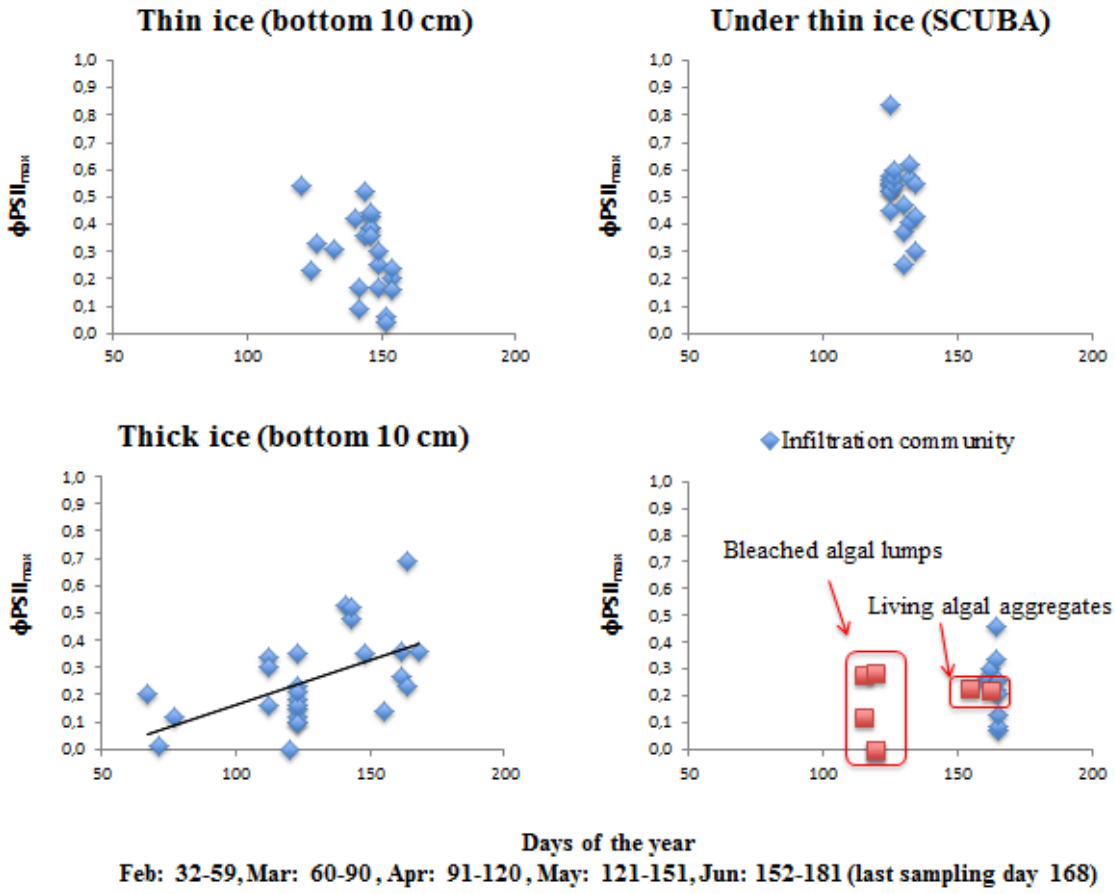

Figure 10: Temporal development of $\Phi PSII_{max}$ for bottom 10 cm of thin (YI) and thick ice (SYI/MYI), water/slush sampled under thin ice close the ridges, the infiltration community encountered on ice-floe 4 and the ice-algal aggregates (partly living/bleached cells found in late April and advected living aggragets later in the season). The illustration shows the great range of $\Phi PSII_{max}$ measurements within each habitat/community.

Photosynthetic response

$\Phi PSII_{max}$ under different environmental conditions are presented in table 3, while averages of $\Phi PSII_{max}$ in the different habitats/communities with corresponding photosynthetic parameters modelled from Phyto-PAM (Eilers and Peeters) and the Jassby and Platt equation are extracted into table 4.

Table 3: Key variables at $\Phi PSII_{max}$ (peak within each habitat). Young Ice (YI) refers to newly formed thin ice (< 30 cm) *e.g.* refrozen leads with only a few centimeters of snow on top. The species occurrence applies for the samples that had following peak dates in $\Phi PSII_{max}$ (within each habitat/community). Chl *a* values are also specific for each habitat at peak date, either made for a subsample or for ice: it is measured from replicate melted core sections (bottom 10 cm). Note that FYI is not the same as "thin ice". The E_{PAR} data is extracted from real (under-ice) and modelled values in each habitats and are to be viewed as approximate values.

Habitat	Community	Snow depth (cm)	Ice thickness (cm)	E_{PAR} (µmol photons m^{-2} s^{-1})	$\Phi PSII_{max}$	Chl a (mg m^{-3})	$\Phi PSII_{max}$ Peak date
SYI/MYI (thick ice)	*Pseudonitzschia* sp., *Navicula* sp., *Nitzschia frigida*	30-40	134	1.4	0.53	0.7	21.05.2015
FYI	*Navicula* sp., *Nitzschia* sp., mixotrophic flagellates, epiphytes	23	133-144	1.4	0.52	11.61	23.05.2015
YI (thin ice)	Photosynthetic ciliate *Mesodinium rubrum*	0-3	14-30	NA	0.52	0.48	05.05.2015
Pressure ridge	*N. frigida, Thalassiosira bioculata*	3	30-47	NA	0.61	26.3	10.05.2015
Infiltration layer	Bacillariophyceae, *Phaeocyctis* sp.	60	NA	143*	0.46	4.46	13.06.2015
Ice-algal aggregated (bleached)	Partly living diatoms (Bacillariophyceae)	40	130	~ 1	0.29	0.07	29.04.2015
Ice-algal aggregates	Bacillariophyceae	NA	NA	NA	0.23	NA	03.06.2015
Water column	*Phaeocystis pouchetii*	40	130	< 1.5	0.66**	5.53	01.06.2015

* Value is calculated from the assumingly absorbed E_{PAR} by the snow layer. Incident E_{PAR} = 709 was subtracted from reflected E_{PAR} = 566. E_{PAR} transmitted few cm below ice at this site was 5.5 µmol photons m^{-2} s^{-1}.

** Published in Assmy *et al.*, 2017

Table 4: Averages and standard deviations (±) of $\Phi PSII_{max}$ and corresponding photosynthetic parameters obtained from RLC with two different equations: Eilers and Peeters (1988) and Jassby and Platt (1976). Webb estimates showed similar parameter values to the Jassby and Platt equation (figure 12-13). E_k is the light saturation parameter ($rETR_{max}/\alpha_{rETR}$) and indicates at which irradiance (E_{PAR}) photosynthesis is saturated (µmol photons m^{-2} s^{-1}). (Note that the species dominance in table 3 does not necessarily apply here. This is due to that light microscopy onboard was restricted only to some samples with good signal, like the highest observed $\Phi PSII_{max}$ in each habitat, table 3).

			Eilers & Peeters (1988)				Jassby & Platt (1976)			
Habitat	**$\bar{\Phi}PSII_{max}$**	**n**	**E_k**	**α_{rETR}**	**$rETR_{max}$**	**n**	**E_k**	**α_{rETR}**	**$rETR_{max}$**	**n**
SYI/MYI (thick ice)	0.28 ± 0.15	17	NA	NA	NA		728 ± 577	0.09 ± 0.04	50 ± 37	8
FYI	0.36 ± 0.20	2	105 ± 28	0.22 ± 0	23 ± 6	2	387 ± 93	0.08 ± 0.01	30 ± 5	2
YI (thin ice)	0.36 ± 0.24	7	NA	NA	NA		140 ± 43	0.15 ± 0.06	23 ± 3	3
Thin ice ridge	0.33 ± 0.17	13	195 ± 90	0.15 ± 0.06	26 ± 9	8	454 ± 192	0.08 ± 0.04	30 ± 12	13
Infiltration layer	0.29 ± 0.08	8	203 ± 75	0.13 ± 0.04	25 ± 8	8	417 ± 135	0.06 ± 0.02	25 ± 9	8
Ice-algal aggregates (bleached)	0.23 ± 0.07	3	NA	NA	NA		NA	NA	NA	
Ice-algal aggregates	0.23 ± 0.01	2	309 ± 19	0.10 ± 0	30 ± 2	2	537 ± 15	0.05 ± 0	27 ± 1	2
Water column	0.59 ± 0.05	12	330 ± 120	0.26 ± 0.03	81 ± 27	12	511 ± 177	0.15 ± 0.02	73 ± 20	12

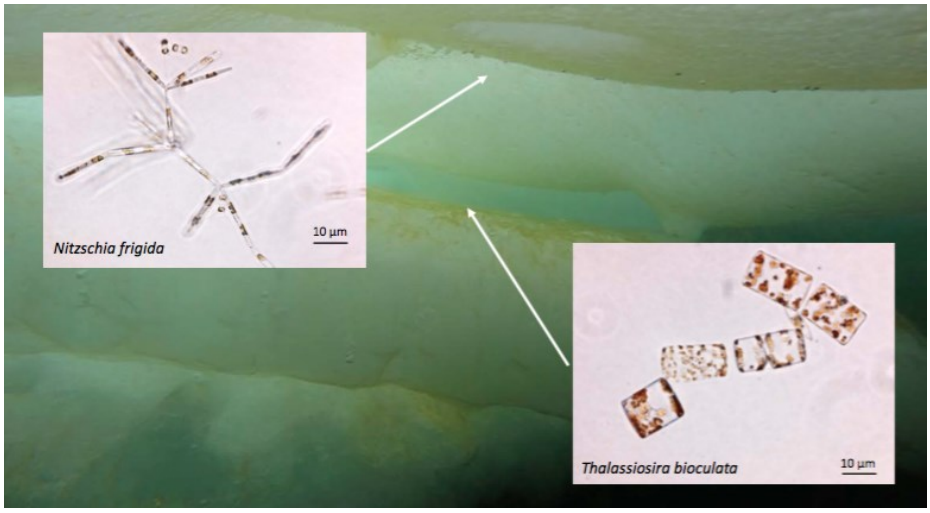

Figure 11: Pressure ice ridge communities sampled in mid-May were dominated by the pennate colony-forming diatom *Nitzschia frigida* at the under-side surfaces of the ice, and the centric diatom *Thalassiosira bioculata* horizontally on top of the ice ledges. (Image by C. J. Mundy and Mar Fernández-Méndes)

Fitting rETR versus E using different mathematical algorithms

The tables on the right side of figure 12-15 show the Eilers and Peeters, Jasby and Platt (and Webb *et al.*) estimates for each fitted rETR curve. Presented below are some examples of different responses and saturation characteristics for the water column, the snow infiltration community and in thin ice communities. The data points in the graphs are the rETR values calculated from the yield output (equation 4) together with the non-linear curves fitted with equation 5-7. The Eilers and Peeters estimates are extracted from the Phyto-PAM output.

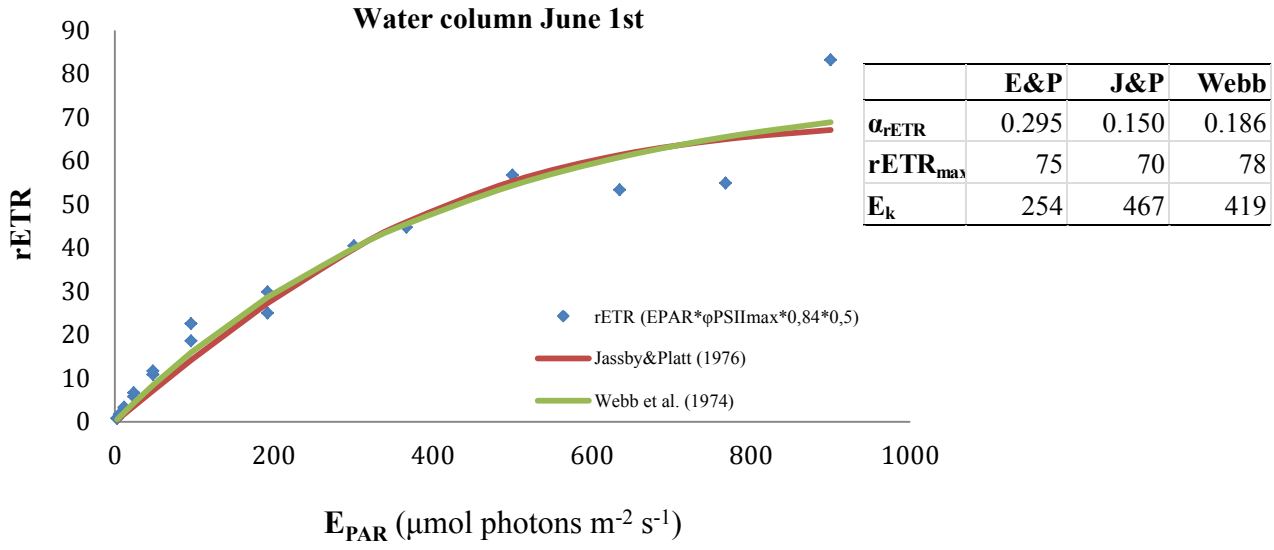

	E&P	J&P	Webb
α_{rETR}	0.295	0.150	0.186
$rETR_{max}$	75	70	78
E_k	254	467	419

Figure 12: Data points showing rETR and fitted curves to data, from a water sample collected with a Niskin bottle at 15 m depth with $\Phi PSII_{max}$ = 0.66, during the *P. pouchetii* bloom. The corresponding table displays the photosynthetic parameters from the three models, equation 5-7. A trend against saturation plateau can be seen at rETR ~ 70.

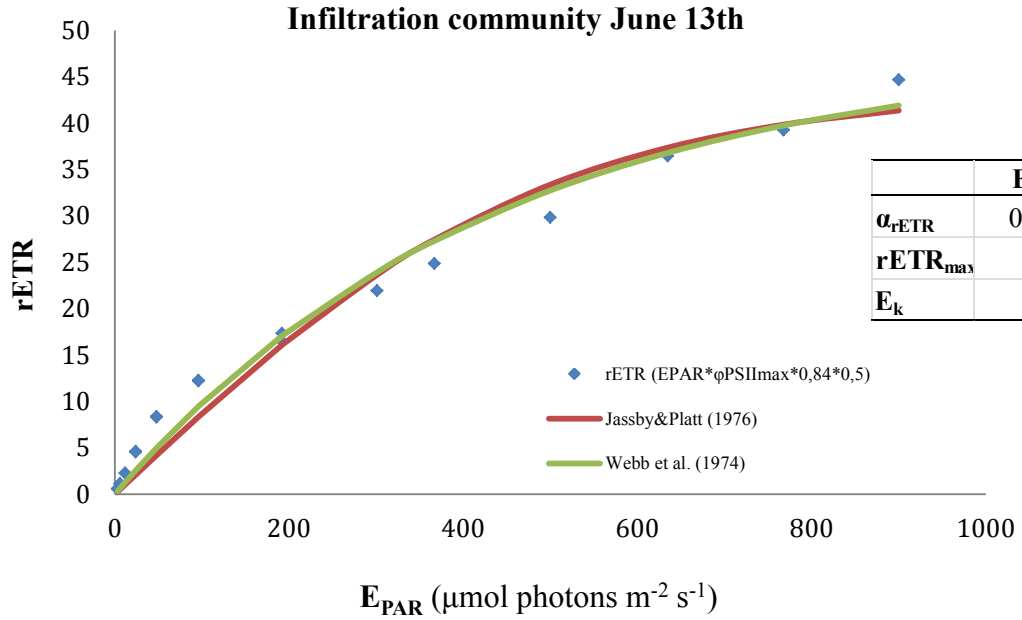

	E&P	J&P	Webb
α_{rETR}	0.210	0.088	0.11
$rETR_{max}$	37	44	48
E_k	174	495	436

Figure 13: Data points showing rETR and fitted curves to data, from a scrape sample from the infiltration community with $\Phi PSII_{max}$ = 0.45. The corresponding table displays the photosynthetic parameters from the three models. A trend against saturation plateau can be seen at rETR ~ 40-45.

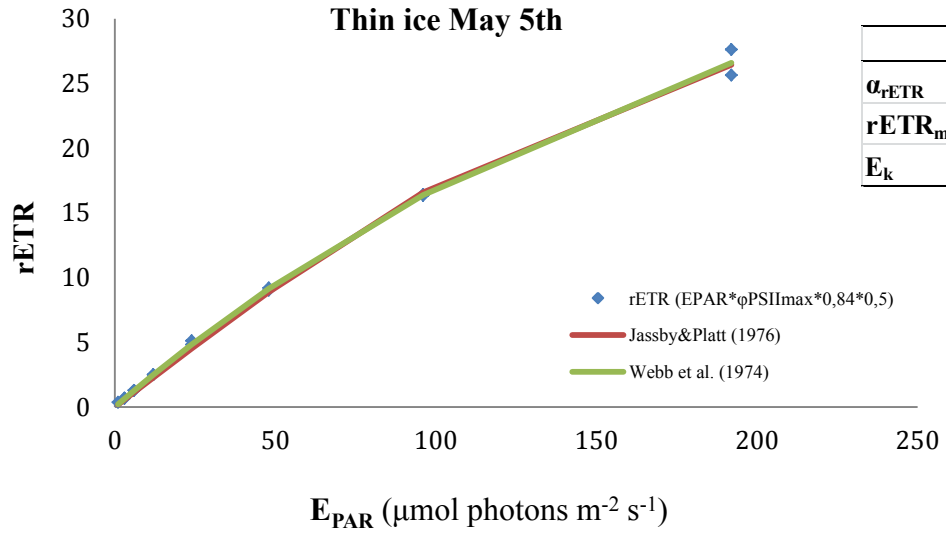

	E&P	J&P	Webb
α_{rETR}	0.228	0.190	0.214
$rETR_{max}$	57	33	44
E_k	250	173	203

Figure 14: Data points showing rETR and fitted curves to data, from a sample collected by divers with a suction pump under thin ice with $\Phi PSII_{max}$ = 0.54. The corresponding table displays the photosynthetic parameters from the three models. There is no trend against a saturation plateau.

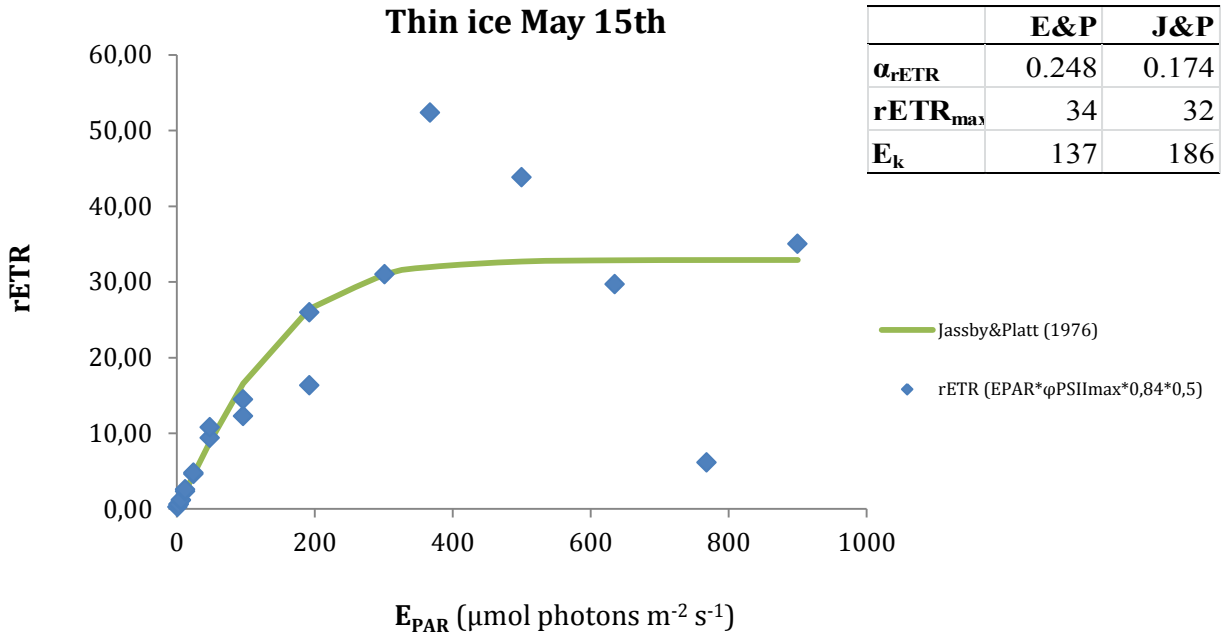

Figure 15: Data points showing rETR and fitted curve to data, from a sample collected by divers with a suction pump under thin ice with $\Phi PSII_{max}$ = 0.61. The corresponding table displays the photosynthetic parameters from the two models. This sample was dominated by the diatom *Thalassiosira bioculata* and reached a clear saturation plateau at rETR = 32.

Discussion

The photosynthetic data obtained from floe 3 and 4 was most suitable at producing reliable yield estimates (*i.e.* low signal/noise) and corresponding rETR values (due to biomass content). The early spring-summer period (April 18th - June 22nd) will therefore be more thoroughly discussed than data from ice-floe 2, when comparing PAM data with environmental observations. Some of the data from the N-ICE2015 expedition has already been published, which will be put in context with the PAM results.

Physical conditions

The mean snow and ice thickness distribution was relatively similar between the different ice-floes. The a higher fraction of thick multi-year ice (MYI) on ice-floe 2 and 3, compared to ice-floe 4 is probably due to the location of ice-floe 4, which was closer to the ice edge where the ice is naturally thinner and more broken up (figure 1, Appendix 2). It is important to address the use of second-year ice (SYI) here as most of the thick ice cores were done for this ice type, although data from this environment is merged together with the MYI habitat as they both represent thick ice with thick snow cover. On ice-floe 3 the thin/young ice (YI) of < 30 cm is evident in figure 5 and corresponds to where much of the thin ice samples for PAM analysis were collected. The ice drilling data (table 2) from defined ice types shows the FYI having ice thickness ranging from 88-125 cm and SYI/MYI from 109-138 cm. The snow depth range was 7-45 cm and 41-47 cm, respectively for these ice types. The negative freeboard on floe 4 might explain how the snow infiltration communities were formed, since heavy snow cover forces the ice to submerge below the sea level, which make algae and phytoplankton able to infiltrate this environment from underneath.

Irradiances were relatively low under the ~ 1 m thick ice both on ice-floes 3 and 4 from March to June. E_{PAR} was less than 2 µmol photons m^{-2} s^{-1} under ice-floe 3, although the irradiance increased gradually from early March to late May (figure 6). On floe 4, the E_{PAR} had reached higher levels: ranging from ~ 1-6 µmol photons m^{-2} s^{-1} (with diurnal variations), due to the increased solar angle and day length that allows more light to penetrate snow and ice. Ice algae are usually adapted to these low-light conditions, with observed photosynthetic activity at irradiances all the way down to 1 µmol photons m^{-2} s^{-1} (Mock & Gradinger, 1999).

In Assmy *et al*., 2017 the modelled light field under defined thin (0.2 m) and thick (1.8 m) ice shows in fact, how the the ice thickness (and snow cover) determines in high degree the amount of E_{PAR} that is transmitted below for photosynthetic utilization: "*The dominant snow-covered thick ice transmitted on average only < 1 % of the incident* E_{PAR}*, Transmittance for thin ice was 20 % on average, ranging from 6.3-42.2 %*".

During N-ICE2015 a ~ 100 m deep winter mixed layer was present indicating high sea ice growth. In addition were freezing of open leads observed in significant amounts (Meyer *et al*., 2017). Open leads are a big resource for sea ice growth due to the thermal properties of sea ice formation (Thomas & Dieckmann, 2010) and impacts the possibilities for colonization by ice algae. From late May and onwards the sea-ice melting started as the ice-floes were closer to the ice edge where the surface mixed layer was thinner and the Atlantic Water shallower (Meyer *et al*., 2017). Advection from warmer water masses like the north going branches of Atlantic Water from Spitsbergen, can in addition lead to under-ice melting and affect the dynamics of sea ice biota by removing nutrients or algae themselves (Stabeno et al., 1998).

In the future it is expected that the precipitation will increase in the Arctic (Bintanja & Selten, 2014), which could have impact on light transmission and on the primary production in ice-covered waters. Despite this, the spectral transmission is important to address, since the snow allows for wavelengths between 400 and 550 nm to pass through, whereas absorption by algae has a peak at around 440 nm (Mundy *et al*., 2007). Ice thickness and ice dynamics (*e.g.* lead formation) are controlling factors for initiating phytoplankton blooms in ice covered waters (Arrigo *et al*., 2012; Assmy *et al*., 2017), and modelling the future Arctic primary production pattern is complex and dependent on many feedback processes.

Responses in $\Phi PSII_{max}$ by the different communities/habitats

Most of the photosynthetic active algae *i.e.* produced best responses to actinic light (displaying high signal/noise in $\Phi PSII_{max}$ and Φ'PSII), were encountered on ice-floe 3 and 4. Number of samples within each habitat/community varied due to "opportunistic" sampling. The $\Phi PSII_{max}$ values are by the findings, defined as low: < 0.3, moderate: 0.3-0.5 and high: > 0.5, indicating different physiological conditions in the different communities or habitats sampled. There was a lot of variation within some communities/habitats (figure 9-10), but the overall range in reliable (not with fluorescence yields that jumped throughout the RLC) $\Phi PSII_{max}$ values varied from 0.1-0.66. The highest responses in terms of $\Phi PSII_{max}$ were found in the thin ice ridge community and in the water column (table 3 and 4). The ice-algal aggregates (Bacillariophyceae) observed in late April were attached to the underside of the ice and sampled by divers, while those observed in June were free-floating and accumulated in core holes (figure 10). These types of aggregates have previously shown low biomass and production compared to ice-algal blooms, but is likely an important food source for ice fauna (Assmy *et al*., 2013). Diatoms (Bacillariophyceae) and *P. pouchetii* mainly dominated the snow infiltration layer/community. *Nitzschia frigida* and *Thalassiosira bioculata* (Bacillariophyceae) made up a specific dominated community composition in some areas of the thin ice ridge in mid-May (figure 11).

For the highest values of $\Phi PSII_{max}$ found in each habitat (table 3), most were from moderate to high, except for the ice-algal aggregates. The ice-algal aggregates had corresponding low chl *a* content and were, in fact, sampled in late April when photosynthetic activity was in recovery. Refrozen leads close to older ice are efficiently colonized (Sakshaug *et al*., 2009), which was the case for the photosynthetic ciliate (contains algal chloroplasts from Cryptophyceae) *Mesodinium rubrum* found in high concentrations under thin ice with high $\Phi PSII_{max}$ = 0.52, early in May. It is a fairly common species in the world oceans and considered being functionally a phytoplankton (Gustafson *et al*., 2000). It can exhibit high photosynthetic rates in addition to take up amino acids and naturally occurring dissolved organic carbon (Smith & Barber, 1979).

Snow infiltration communities are formed on top of the sea ice (snow-ice interface) when the weight of the snow forces the ice below sea level (negative freeboard). These communities have been considered common in the Southern Ocean, but have recently become more prevalent in the Arctic, possibly by the changes in the Arctic pack ice (McMinn & Hegseth,

2004; Sakshaug *et al*., 2009). $\Phi PSII_{max}$ average values of 0.29 ± 0.08 were similar but a bit higher than those encountered by McMinn & Hegseth, 2004 ($\Phi PSII_{max}$ ~ 0.25). One could argue that table 3, having high peak values for many of the habitats, might be incorrect at times. For example in SYI/MYI the $\Phi PSII_{max}$ = 0.53, but the chl *a* concentration is only 0.7 mg m^{-3}. Although the PAM instrument is not (in theory) dependent on the concentration of algae to measure fluorescence, it was clear that low biomass led to poor production of RLC data points. Many of the RLC produced in the melted ice samples were not always saturated or had clear response in utilizing the actinic light. Since Phyto-PAM is mainly designed to measure chl *a* fluorescence in phytoplankton solutions, this might be a source of error, or the melted ice could contain fluorescing particles. In fact, detritus is an important sediment component in sea ice of high latitudes (Hebbeln, 2000). A single measurement done with a Flow-Cytometer in the defined ice types (SYI/MYI, FYI and YI) from the expedition showed that detritus was found in amounts compared to those of ice algae, which might be a source of interference with the fluorescence signal (Olsen L. pers. Com).

As for the horizontal and vertical ice blocks dominated by the diatoms *Thalassiosira bioculata* and *Nitzschia frigida*, respectively, high $\Phi PSII_{max}$ and biomass content (seen in figure 11) was in line with each other. The ridge community itself had moderate averages in $\Phi PSII_{max}$. Polysaccharides exuded by *N. frigida* in contrast to *T. bioculata* might be an efficient way to stay attached to the ice surface. Pressure ridges can reach several meters below the sea surface and form complex structures for ice algae to settle (Sakshaug *et al*., 2009). These communities showed to be flourishing photosynthetically and in biomass ($\Phi PSII_{max}$ ~ 0.3-0.6 and < 26 mg chl *a* m^{-3}).

The *P. pouchetii* bloom had high $\Phi PSII_{max}$ = 0.66, sampled at 20-40 m depths. As supported in Assmy *et al*. (2017), *P. pouchetii* is able to photo-acclimate to varying irradiances, *e.g.* by increasing their absorption of blue-green light (SoHoo *et al*., 1987). This type of adaptation walks hand-in-hand with the prymnesiophyte's success and distribution in the vast oceans.

As for the species composition, no complete taxonomical data set has been finished for the N-ICE2015 expedition at time of writing. It is therefore a very general species composition

observed at the $\Phi PSII_{max}$ peak days in the different habitats that is provided in table 3. In addition, data obtained from single measurements with the Flow Cytometer (Olsen L. pers. Com) in the defined ice types (MYI, FYI and YI) showed that the presence of *Navicula* sp. were more common in FYI and YI, than in MYI. *Nitzschia* sp. mostly dominated the MYI, which is consistent what we know about this key species (Sakshaug *et al*., 2009). In regards to the biomass for each $\Phi PSII_{max}$ in the different habitats (chl *a*, table 3), it is assumable that replicate ice cores measured for chl *a* content are low even when $\Phi PSII_{max}$ is high (YI and MYI) due to the spatial patchiness of ice algae within ice structures and under the sea ice. Chl *a* values were however, high in the FYI, pressure ridge communities and in the water column.

Photosynthetic parameters: α_{rETR} and E_k

Since photosynthetic responses obtained with the PAM instrument were in general very low ($\Phi PSII_{max} < 0.3$) up until the shift between April and March (figure 9; RLC: Appendix I), no photosynthetic parameters, except for the $\Phi PSII_{max}$, could be obtained because the samples did not reach a saturation plateau (figure 15) or the signal/noise was too low to be interpreted as a clear photosynthetic response. Only for the thin ice habitat modelled in table 4 the E_k estimated with Jassby and Platt was at "physiological" values ($E_k = 140 \pm 43$). This is because low-light acclimated cells that inhabit sea ice are expected to have low E_k (saturated at low irradiances) and higher α_{rETR} (efficient utilization of low light) values, although these parameters changes throughout the photo-acclimation period (Manes & Gradinger, 2009). E_k especially, indicates the photo-acclimation status (Sakshaug *et al*., 2009) and is a function of α_{rETR} and $rETR_{max}$. Using RLC it would be preferable to ensure that the $rETR_{max}$ is determined (*i.e.* so we have high enough actinic light levels and enough data points to estimate a plateau) to make good estimates for E_k. The choice of mathematical functions is reflected in the photosynthetic parameters α_{rETR} and E_k, but the parameters are also spectrally dependent (Sakshaug *et al*., 2009).

The water column showed highest average in $\Phi PSII_{max}$ with little variation and high signal/noise, clearly sticking out from the more moderate values in thin/young ice, thin ice ridge communities and FYI (table 4). The poorest signal was found in the ice-algal aggregates, which contained a large fraction of dead and moribund algae. The bottom communities of SYI/MYI showed almost moderate $\Phi PSII_{max}$ values (average of 0.28 ± 0.15)

and were the habitat sampled most and over longest time from March to June. This is closer to December values than March-May values of $\Phi PSII_{max}$ shown in bottom communities in Manes & Gradinger (2009), which were 0.33-0.43 and 0.47-0.59, respectively. Despite low average of $\Phi PSII_{max}$ the temporal development of $\Phi PSII_{max}$ in SYI/MYI had a significant increase during the expedition (regression analysis, Appendix I), showing the expected development for bottom ice communities towards spring/summer with acclimation to increased irradiances under ice (Manes & Gradinger, 2009). The bleached and partly active ice-algal aggregates were not possible to extract photosynthetic information from besides the $\Phi PSII_{max}$ due to low signal/noise and that no saturating plateau was seen during non-linear curve fitting. The living ice-algal aggregates were however possible to withdraw photosynthetic parameters from. As for all of the habitats/communities, they also showed averages that were high in α_{rETR} and low in E_k with the Eilers and Peeters equation and low in α_{rETR} and high in E_k with the Jassby and Platt equation (table 4).

rETR calculations with different algorithms

The light saturation parameter E_k is an interesting feature in these experiments. Phyto-PAM estimates from the Eilers and Peeters (1988) equation showed a higher α_{rETR} and lower E_k than the Jassby and Platt (1976) and Webb *et al.* (1974) equations, that showed the opposite trend (figure 12-13). In figure 14, no plateau is forming at the low irradiances set for the RLC, and therefore the E_k cannot be estimated properly or used for physiological interpretation. Here, the parameter values in the side figure are also quite similar between the different equations. In the rETR-curve showing a clear light saturating plateau (figure 15), the parameters obtained from Eilers and Peeters and Jassby and Platt equations are quite similar (except for α_{rETR}), indicating that these two ways of curve fitting rETR against E might not be so different when the sample first reaches saturating irradiances and is responding well to actinic light. The non-saturating feature of many of the samples may have led to over-estimation of the photosynthetic parameters such as E_k, which can be seen in table 4. It seems that, in order to reach $rETR_{max}$ the irradiances used (E_{PAR} < 900 μmol photons m^{-2} s^{-1}) may not be high enough, or the RLC might not be a natural way for the cells to respond to actinic light. This might be due to the fact that the ice algae are low-light acclimated and might need "time" to adjust to increasing irradiances. The Eiler and Peeters (1988) model (which has a

rational equation) was used when Phyto-PAM did estimation of α_{rETR} and $rETR_{max}$ where the Z_{off}-function had been used. These estimates were not obtained for all samples. Instead the Jassby and Platt (1976) equation was used and compared with the Webb *et al*. (1974) model, which seemed to be very similar to each other (figure 12-13). Number of data points has an important impact on the curve fitting, and as the irradiance increases, the data points scatter more due to NPQ (figure 12 and 15). There should for example be > 6 data points to generate α_{rETR} (linear part of photosynthesis).

Challenges

The melting process with adding (1:2) parts filtered seawater (by volume) to avoid osmotic shock is supported by literature (Ryan *et al.*, 2004). The melting time however, might be one of the most important factors causing stress to the ice-melted cells due to the rapid change of their environment in close-to room temperature aboard the ship. This was unfortunately the outcome of heavy work load and sparse time. The fluorescence data (F_o, F_o', F_m, F_m') had low signal/noise, especially in the beginning of sampling (March), mainly due to low biomass and might also be a result of the melting procedure or the combination of these. The biomass might simply have been too low for the instrument to detect F_o and F_m, as no ice algae was clearly observed until late April/beginning of May. The dark-acclimation time is another factor that might have been causing the noise in the data, due to re-oxidation processes occuring over long time, which logistically were challenging to overcome due to sampling schedule. Although the detection limit of active chl *a* is well below 0.5 mg m^{-3} for Phyto-PAM (Waltz, 2003), the samples where high auto-gain was set (due to low biomass or cells unable to fluoresce) before RLC, the signal/noise led to scattered data that was not seen as "reliable" in terms of photosynthetic response. The PHYTO-ED unit is optimized for maximal sensitivity at minimal background fluorescence (Waltz, 2003), but it is possible that its more specific use in analyzing surface water phytoplankton samples does not fit well with melted sea-ice samples. The auto-corrective Zoff function seemed however, to be the best and most consistent way to measure the samples where the biomass was not too low. This is likely due to that the Zoff function decreases the signal/noise ratio before starting the measurement (Waltz, 2003). Dilution of cell density might also have an effect on the signal strength; especially where filtrated seawater was added to the sampled ice. Where background fluorescences was corrected in the aftermath of producing RLC, the gain was usually high (~ 20), which naturally caused a low signal/noise. At times, the fluorescence yields ($\Phi PSII_{max}$

and Φ'PSII) corrected with a blank were negative or above the theoretical value 0.83. These data had to be discarded, as it was not possible to interpret the values as ecologically viable or produce any rETR parameter estimates. It is recommended to use the Zoff function for similar studies where the sample water is assumed to not contain any significant amount of fluorescing particles (*e.g.* humic acids in natural surface waters). The software Phyto-Win had a tendency to crash and mix up the irradiance setting for the RLC which led to some RLC starting with 12 μmol photons m^{-2} s^{-1} instead of 1 or 3. This did not seem to have too much of an impact for the samples with good signal (reaching saturating plataeu). The sampling was in addition done opportunistically for some environments, *e.g*. those done by divers where they observed visible communities and visible high densities of algae (colored snow) in the snow-infiltration layers. For several samples high fluorescence background signal was detected when the filtrated blank was used to correct after RLC measurement. This might indicate that the method can have caused the cells to burst inside the filter, causing a leak of pigments into the blank sample and therefore a high fluorescence signal due to auto-fluorescence by dead cells.

Conclusion

Although the $\Phi PSII_{max}$ values varied greatly within some of the habitats (*e.g.* snow infiltration community), it seems to be in accordance with photosynthetic activity (measured chl *a* content) and visible observations of active assemblages in the snow infiltration layer, the ridges and under thin ice and bottom 10 cm of FYI. The question on how well the photosynthetic parameters α_{rETR}, $rETR_{max}$ and E_k gained from RLC in Phyto-PAM measurements, gives an insight into the physiological states of the collected sea-ice algae and phytoplankton, is complex and depends on many factors such as chl *a* emission signal (fluorescence) to noise ratio, saturating flash duration (needs to be long enough to get required data points for F_m), the actual state of the algal cells in the sample (dead or living cells, if able to perform photosynthesis at all, methodological challenges (sampling and melting procedures, light acclimation time etc.), to mention some. There is still a clear response, however using RLC where the biomass is relatively high (> 0.5 chl *a* mg m^{-3}). Using the Z_{off} function is to recommend since it is a more straightforward way of determine $\Phi PSII_{max}$. Interesting findings with good photosynthetic signal and reliable rETR-E curves were however made with the high activity within some communities: thin ice, ridge communities and the predominant *P. pouchetii* bloom in the water column. The bloom was sustained by frequent lead formation and is a clear example for the opportunistic way of living high Arctic algae exhibit, adapting their photosynthetic rates to increasing irradiances.

Cruise expeditions are challenging, especially in the high Arctic with unforeseen weather changes and logistics. During N-ICE2015 there was constant juggling between tasks and many people involved in the same measurements as the crew exchanged several times. Low biomass/sensitivity of Phyto-PAM instrument and experimental protocols with small changes during the expedition did have some impact on the measurements. A need for strict protocols and control of melting temperatures etc. are necessary to provide larger datasets for modelling photosynthetic characteristics in high Arctic ice algae and phytoplankton in the future.

References

1. Arrigo, K. R & Thomas, D. N (2004). Large scale importance of sea ice biology in the Southern Ocean. *Antarctic Science 16*, 471–486. DOI: 10.1017/S0954102004002263

2. Arrigo, K. R., Perovich, D. K., Pickart, R. S., Brown, Z. W., Van Dijken, G. L., Lowry, K. E., ... & Swift, J. H. (2012). Massive phytoplankton blooms under Arctic sea ice. *Science 336*(6087), 1408-1408. DOI: 10.1126/science.1215065

3. Arrigo, K. R. (2014). Sea ice ecosystems. *Annual review of marine science 6*, 439-46. DOI: 10.1146/annurev-marine-010213

4. Assmy, P., Ehn, J. K., Fernández-Méndez, M., Hop, H., Katlein, C., Sundfjord, A., ... & Granskog, M. A. (2013). Floating ice-algal aggregates below melting Arctic sea ice. *PLoS One 8*(10), e76599. DOI: 10.1371/journal.pone.0076599

5. Assmy, P., Fernández-Méndes, M., Duarte, P., Meyer, A., Randelhoff, A., Mundy, C. J., Olsen, L., … & Granskog, M. A. (2017). Leads in the Arctic pack ice enable early phytoplankton blooms below snow-covered sea ice. *Scientific Reports 7*, 40850. DOI: 10.1038/srep40850

6. Baker, N. R., & Oxborough, K. (2004). Chlorophyll fluorescence as a probe of photosynthetic productivity. In *Chlorophyll* a *Fluorescence* (65-82). Springer Netherlands. DOI: 10.1007/978-1-4020-3218-9_3

7. Beer, S. & Ilan, M. (1998). In situ measurements of photosynthetic irradiance responses of two Red Sea sponges growing under dim light conditions. *Marine Biology 131*, 613-617. DOI: 10.1007/s002270050353

8. Bintanja, R. & Selten, F. M. (2014). Future increases in Arctic precipitation linked to local evaporation and sea-ice retreat. *Nature 509*(7501), 479-482.

9. Braun, G. Z & Braun, B. Z. (1974). *Light Absorption, Emission and Photosynthesis*. W.D.P. Stewart (Ed.)*, Algal physiology and biochemistry.* Blackwell Scientific Publications, Oxford.

10. Eilers, P. H. C. & Peeters, J. C. H. (1988). A model for the relationship between light intensity and the rate of photosynthesis in phytoplankton. *Ecological modelling 42*, 199–215. DOI: 10.1016/0304-3800(88)90057-9

11. Falkowski, P. G. & LaRoche, J. (1991). Acclimation to spectral irradiance in algae. *Journal of Phycology 27*(1), 8-14. DOI: 10.1111/j.0022-3646.1991.00008.x

12. Genty, B., Briantais, J. M. & Baker, N. R. (1989). The relationship between the quantum yield of photosynthetic electron-transport and quenching of chlorophyll fluorescence. *Biochimica et Biophysica Acta 990*(1), 87-92. DOI: 10.1016/S0304-4165(89)80016-9

13. Gilbert, M., Wilhelm, C., & Richter, M. (2000). Bio-optical modelling of oxygen evolution using in vivo fluorescence: Comparison of measured and calculated photosynthesis/irradiance (PI) curves in four representative phytoplankton species. *Journal of Plant Physiology 157*(3), 307-314. DOI: 10.1016/S0176-1617(00)80052-8

14. Gradinger, R. (2009). Sea-ice algae: Major contributors to primary production and algal biomass in the Chukchi and Beaufort Seas during May/June 2002. *Deep Sea Research Part II: Topical Studies in Oceanography 56*(17), 1201-1212. DOI: 10.1016/j.dsr2.2008.10.016

15. Gustafson, D. E., Stoecker, D. K., Johnson, M. D., Van Heukelem, W. F. & Sneider, K. (2000). Cryptophyte algae are robbed of their organelles by the marine ciliate *Mesodinium rubrum*. *Nature 405*(6790), 1049-1052. DOI: 10.1038/35016570

16. Hancke, T. B., Johnsen, G. & Sakshaug, E. (2008). Rate of O_2-production derived from Pulse-Aplitude-Modulated fluorescence: Testing three bio-optical approaches against measured O_2 production rate. *Journal of Phycology 44*, 803-813. DOI: 10.1111/j.1529-8817.2008.00509.x

17. Hebbeln, D. (2000). Flux of ice-rafted detritus from sea ice in the Fram Strait. *Deep Sea Research Part II: Topical Studies in Oceanography 47*(9), 1773-1790. DOI: 10.1016/S0967-0645(00)00006-0

18. Jassby, A. D., & T. Platt. (1976). Mathematical formulation of the relationship between photosynthesis and light for phytoplankton. *Limnology and Oceanography 21*(4), 540-547. DOI: 10.4319/lo.1976.21.4.0540

19. Johnsen, G. & Sakshaug, E. (2007). Biooptical characteristics of PSII and PSI in 33 species (13 pigment groups) of marine phytoplankton, and the relevance for pulse-amplitude-modulated and fast-repetition-rate fluorometry. *Journal of Phycology 43*(6), 1236-1251. DOI: 10.1111/j.1529-8817.2007.00422.x

20. Knap, A. H., Michaels, A., Close, A. R., Ducklow, H. & Dickson, A. G. (1996). Protocols for the joint global ocean flux study (JGOFS) core measurements. *JGOFS Report 19*, 118-122.

21. Lederman, T. C. & Tett, P. (1981). Problems in modelling the photosynthesis-light relationship for phytoplankton. *Botanica Marina 24*(3), 125-134. DOI: 10.1515/botm.1981.24.3.125

22. Leu, E., Mundy, C. J., Assmy, P., Campbell, K., Gabrielsen, T. M., Gosselin, M., Juul-Pedersen T. & Gradinger R. (2015). Arctic spring awakening-steering principles behind the phenology of vernal ice algal blooms. *Progress in Oceanography 139*, 151-170. DOI: 10.1016/j.pocean.2015.07.012

23. Magnusson, G. (1997). Diurnal measurements of F_v/F_m used to improve productivity estimates in macroalgae. *Marine Biology 130*(2), 203-208. DOI: 10.1007/s002270050239

24. Manes, S. S. & Gradinger, R. (2009). Small scale vertical gradients of Arctic ice algal photophysiological properties. *Photosynthesis research 102*(1), 53-66. DOI: 10.1007/s11120-009-9489-0

25. Maxwell, K. & Johnson, G. N. (2000). Chlorophyll fluorescence - a practical guide. *Journal of Experimental Botany 51* (345), 659-668. DOI: 10.1093/jexbot/51.345.659

26. McMinn, A. & Hegseth, E. N. (2004). Quantum yield and photosynthetic parameters of marine microalgae from the southern Arctic Ocean, Svalbard. *Journal of the Marine Biological Association of the United Kingdom 84*, 865–871; DOI: 10.1017/S0025315404010112h

27. Meyer, A., Sundfjord, A., Fer, I., Provost, C., Villacieros Robineau, N., Koenig, Z., Onarheim, I. H., Smedsrud, L. H., Duarte, P., Dodd, P. A., Graham, R. M., Schmidtko, S. & Kauko, H. M. (2017). Winter to summer oceanographic observations in the Arctic Ocean north of Svalbard. *Journal of Geophysical Research: Oceans*. Accepted Author Manuscript. DOI: 10.1002/2016JC012391

28. Mock, T. & Gradinger, R. (1999). Determination of Arctic ice algal production with a new in situ incubation technique. *Marine Ecology Progress Series 177*, 15-26. DOI: 10.3354/meps177015

29. Müller, P., Li, X. P., & Niyogi, K. K. (2001). Non-photochemical quenching. A response to excess light energy. *Plant physiology 125*(4), 1558-1566. DOI: 10.1104/pp.125.4.1558

30. Mundy, C. J., Ehn, J. K., Barber, D. G. & Michel, C. (2007). Influence of snow cover and algae on the spectral dependence of transmitted irradiance through Arctic landfast first-year sea ice. *Journal of Geophysical Research*: *Oceans 112*(C3). DOI: 10.1029/2006JC003683

31. Nitschke, U., Connan, S. & Stengel, D. B. (2012). Chlorophyll *a* fluorescence responses of temperate Phaeophyceae under submersion and emersion regimes: a comparison of rapid and steady-state light curves. *Photosynthesis Research 114*, 29-42. DOI: 10.1007/s11120-012-9776-z

32. Ralph, P. J. & Gademann, R. (2005). Rapid light curves: A powerful tool to assess photosynthetic activity. *Aquatic Botany 82*, 222-37. DOI: 10.1016/j.aquabot.2005.02.006

33. Roy, S., Llewellyn, C. A., Egeland, E. S. & Johnsen, G. (2011). *Phytoplankton pigments: Characterization, chemotaxonomy and applications in oceanography*. Cambridge University Press. ISBN: 978-1-107-00066-7

34. Rösel, A., Polashenski, C. M., Liston, G. E., King, J. A., Nicolaus, M., Gallet, J., … & Granskog, M. A. (2016a). *N-ICE2015 snow depth data with Magna Probe* [Data set]. Norwegian Polar Institute. DOI: 10.21334/npolar.2016.3d72756d

35. Rösel, A., Divine, D., King, J. A., Nicolaus, M., Spreen, G., Itkin, P., … & Granskog, M. A. (2016b). *N-ICE2015 total (snow and ice) thickness data from EM31* [Data set]. Norwegian Polar Institute. DOI: 10.21334/npolar.2016.70352512

36. Ryan, K. G., Ralph P. & McMinn A. (2004). Acclimation of Antarctic bottom-ice algal communities to lowered salinities during melting. *Polar Biology* 27: 679-686, DOI: 10/1007/s00300-004-0636-y

37. Sakshaug E., Johnsen G., Kovacs K. M. (2009). *Ecosystem Barents Sea*. Trondheim, Tapir Academic Press. ISBN: 978-82-519-2461-0

38. Schreiber, U., Endo, T., Mi, H., & Asada, K. (1995). Quenching analysis of chlorophyll fluorescence by the saturation pulse method: particular aspects relating to the study of eukaryotic algae and cyanobacteria. *Plant and Cell Physiology 36*(5), 873-882. DOI: 10.1093/oxfordjournals.pcp.a078833

39. Smetacek, V. & Nicol, S. (2005). Polar ocean ecosystems in a changing world. *Nature 437*, 362-368. DOI: 10.1038/nature04161

40. Smith, W. O. & Barber, R. T. (1979). A carbon budget for the autotrophic ciliate Mesodinium rubrum. *Journal of Phycology 15*(1), 27-33. DOI: 10.1111/j.1529-8817.1979.tb02957.x

41. Smith, Jr. W. O., & Sakshaug, E. (1990). Chapt. 9: *Polar phytoplankton. Polar oceanography, Part B: Chemistry, biology and geology*, 477-525. ISBN: 0-12-653032-7

42. Stabeno, P. J., Schumacher, J. D., Davis, R. F. & Napp, J. M. (1998). Under-ice observations of water column temperature, salinity and spring phytoplankton dynamics: Eastern Bering Sea shelf. Journal of *Marine Research 56*(1), 239-255. DOI: 10.1357/002224098321836172

43. Suggett, D. J., Borowitzka, M. A. & Prášil, O. (2010). *Chlorophyll a fluorescence in aquatic sciences: methods and applications. Developments in Applied Phycology*, v. 4. ISBN: 978-90-481-9268-7

44. Syvertsen E. E. (1991). Ice algae in the Barents Sea: types of assemblages, origin, fate and role in the ice-edge phytoplankton bloom. *Polar Research 10(*1), 277-288. Published online 16th of December 2016. DOI: 10.3402/polar.v10i1.6746

45. Taskjelle, T., Hudson, S. R., Pavlov, A., & Granskog, M. A. (2016). *N-ICE2015 surface and under-ice spectral shortwave radiation data* [Data set]. Norwegian Polar Institute. DOI: 10.21334/npolar.2016.9089792e

46. Thomas, D. N. & Dieckmann, G. S. (2010). *Sea ice* (2nd ed.) United Kingdom: Blackwell Publishing Ltd. ISBN: 978-1-4051-8580-6

47. Walz, H. (2003). *Phytoplankton analyzer Phyto-PAM and Phyto-Win software V 1.45, system components and principles of operation* (2nd ed.) Effeltrich, Germany. URL: http://www.walz.com/downloads/manuals/phyto-pam/phyto_4e.pdf

48. Webb, W. L., Newton, M. & Starr, D. (1974). Carbon dioxide exchange of *Alnus rubra*. *Oecologia 17*, 281-291. DOI: 10.1007/BF00345747

Appendix 1 – Rapid Light Curves

RLC quality of all samples analyzed with Phyto-PAM. Explaination of RLC column:

(-): a relatively noisy RLC was produced

(+): the RLC had a *tendency* of reaching a saturating plateau (*i.e.* $rETR_{max}$)

(++): the RLC has all parameters obtained (table 4) from reaching a clear plateau.

Date of sampling	Type/classification	$\Phi PSII_{max}$	RLC
08.03.2015	MYI/thick ice	0,18	-
18.03.2015	MYI/thick ice	0,12	-
22.04.2015	MYI/thick ice	0,34	-
22.04.2015	MYI/thick ice	0,30	-
22.04.2015	MYI/thick ice	0,22	-
25.04.2015	Algal lumps (bleached)	0,28	+
25.04.2015	Algal lumps (bleached)	0,13	+
29.04.2015	Algal lumps (bleached)	0,29	-
30.04.2015	MYI/thick ice	0,53	-
30.04.2015	MYI/thick ice	0,33	-
30.04.2015	MYI/thick ice	0,54	-
30.04.2015	MYI/thick ice	0,33	-
30.04.2015	MYI/thick ice	0,12	+
30.04.2015	MYI/thick ice	0,18	-
30.04.2015	MYI/thick ice	0,34	+
30.04.2015	MYI/thick ice	0,23	-
04.05.2015	YI/thin ice	0,16	-
04.05.2015	YI/thin ice	0,16	-
04.05.2015	YI/thin ice	0,18	-
04.05.2015	YI/thin ice	0,23	-
05.05.2015	YI/thin ice	0,52	-
05.05.2015	YI/thin ice	0,45	+
05.05.2015	YI/thin ice	0,84	+
06.05.2015	YI/thin ice	0,54	+
06.05.2015	YI/thin ice	0,54	+
06.05.2015	YI/thin ice	0,57	+
06.05.2015	YI/thin ice pressure ridge	0,60	+
06.05.2015	YI/thin ice	0,33	-
10.05.2015	YI/thin ice pressure ridge	0,54	+
10.05.2015	YI/thin ice pressure ridge	0,61	+
10.05.2015	YI/thin ice	0,47	-
10.05.2015	YI/thin ice	0,25	-
10.05.2015	YI/thin ice	0,37	-
12.05.2015	YI/thin ice pressure ridge	0,17	-

12.05.2015	YI/thin ice	0,57	+
12.05.2015	YI/thin ice	0,62	+
12.05.2015	YI/thin ice	0,41	-
12.05.2015	YI/thin ice	0,30	+
14.05.2015	YI/thin ice pressure ridge	0,48	++
14.05.2015	YI/thin ice pressure ridge	0,47	++
14.05.2015	YI/thin ice pressure ridge	0,49	+
14.05.2015	YI/thin ice	0,55	+
14.05.2015	YI/thin ice	0,43	++
14.05.2015	YI/thin ice	0,30	-
15.05.2015	YI/thin ice	0,51	+
15.05.2015	YI/thin ice	0,56	+
15.05.2015	YI/thin ice	0,60	++
15.05.2015	YI/thin ice	0,50	+
18.05.2015	YI/thin ice pressure ridge	0,35	++
18.05.2015	YI/thin ice pressure ridge	0,28	++
18.05.2015	YI/thin ice pressure ridge	0,19	++
18.05.2015	YI/thin ice pressure ridge	0,28	++
20.05.2015	YI/thin ice	0,42	++
21.05.2015	MYI/thick ice	0,53	+
22.05.2015	YI/thin ice	0,09	-
22.05.2015	YI/thin ice	0,17	+
23.05.2015	FYI	0,48	+
23.05.2015	FYI	0,52	++
24.05.2015	YI/thin ice	0,36	+
24.05.2015	YI/thin ice	0,52	+
25.05.2015	Water column (5-15 m depth)	0,48	+
26.05.2015	YI/thin ice	0,39	++
26.05.2015	YI/thin ice	0,43	++
26.05.2015	YI/thin ice	0,39	++
26.05.2015	YI/thin ice	0,44	++
26.05.2015	YI/thin ice	0,36	++
28.05.2015	YI/thin ice pressure ridge	0,10	-
28.05.2015	YI/thin ice pressure ridge	0,18	+
28.05.2015	FYI	0,08	-
29.05.2015	YI/thin ice	0,25	+
29.05.2015	YI/thin ice	0,17	-
29.05.2015	YI/thin ice	0,30	+
29.05.2015	MYI/thick ice	0,28	-
31.05.2015	YI/thin ice pressure ridge	0,13	+
31.05.2015	YI/thin ice pressure ridge	0,07	-
01.06.2015	Water column (5-15 m depth)	0,64	+
01.06.2015	Water column (5-15 m depth)	0,66	++
02.06.2015	Water column (5-15 m depth)	0,60	+

02.06.2015	Water column (5-15 m depth)	0,61	+
02.06.2015	Water column (5-15 m depth)	0,60	+
03.06.2015	Algal aggregates (advected)	0,23	++
04.06.2015	MYI/thick ice	0,14	+
06.06.2015	Water column (5-15 m depth)	0,65	+
09.06.2015	Snow infiltration community	0,26	+
10.06.2015	Snow infiltration community	0,26	+
11.06.2015	Snow infiltration community	0,30	+
11.06.2015	Water column (5-15 m depth)	0,52	-
11.06.2015	Water column (5-15 m depth)	0,53	+
11.06.2015	Water column (5-15 m depth)	0,58	+
11.06.2015	Water column (5-15 m depth)	0,64	+
11.06.2015	Algal aggregates (advected)	0,22	+
12.06.2015	MYI/thick ice	0,27	+
12.06.2015	Water column (5-15 m depth)	0,59	-
13.06.2015	MYI/thick ice	0,26	+
13.06.2015	Snow infiltration community	0,46	++
13.06.2015	Snow infiltration community	0,33	++
13.06.2015	Snow infiltration community	0,22	+
14.06.2015	MYI/thick ice	0,62	+
14.06.2015	Snow infiltration community	0,07	-
14.06.2015	Snow infiltration community	0,09	-
14.06.2015	Snow infiltration community	0,21	+
14.06.2015	Snow infiltration community	0,26	+
14.06.2015	Snow infiltration community	0,13	-
14.06.2015	Water column (5-15 m depth)	0,89	-
16.06.2015	Water column (5-15 m depth)	0,11	+
18.06.2015	MYI/thick ice	0,06	+

Regression on $\Phi PSII_{max}$ temporal development in thick ice (MYI) (by Duarte P.). Significant increase in $\Phi PSII_{max}$ over time.

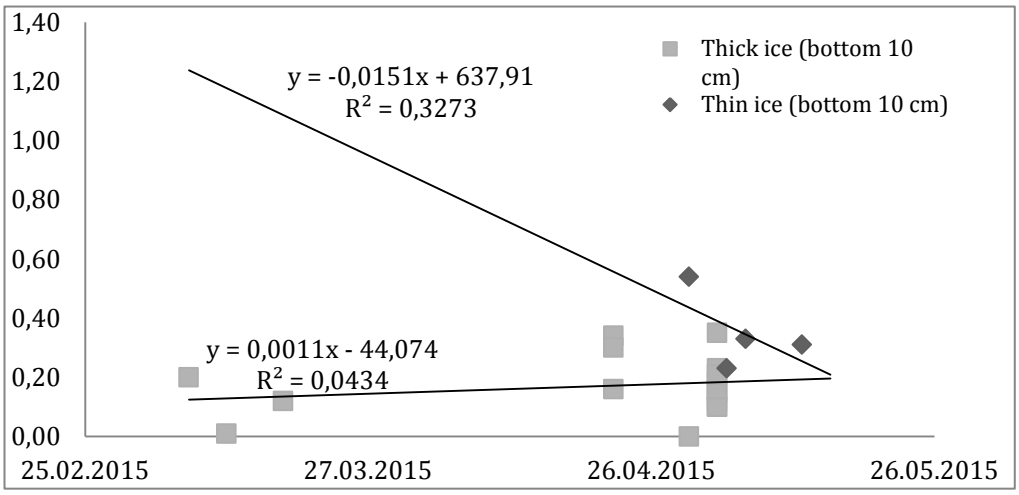

SUMMARY OUTPUT								
Regression Statistics								
Multiple R	0,392064627							
R Square	0,153714671							
Adjusted R Squ	0,103933181							
Standard Error	0,142092661							
Observations	19							
ANOVA								
	df	*SS*	*MS*	*F*	*Significance F*			
Regression	1	0,062343435	0,062343435	3,087787682	0,096875177			
Residual	17	0,343235513	0,020190324					
Total	18	0,405578947						
	Coefficients	Standard Error	t Stat	P-value	Lower 95%	Upper 95%	Lower 95.0%	Upper 95.0
Intercept	242,9771003	138,104229	1,7593748	0,096496868	-48,39735345	534,3515541	-48,39735345	534,3516
X Variable 1	-0,005757949	0,003276756	-1,757210199	0,096875177	-0,0126713	0,001155402	-0,0126713	0,001155

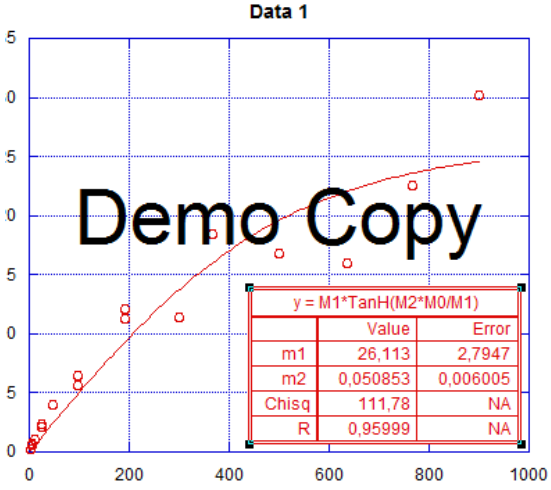

Example from non-linear curve fitting output with KaleidaGraph (demo) with the J&P equation, m1 = $rETR_{max}$ and m2 = α_{rETR}.

Appendix 2 – Miscellaneous

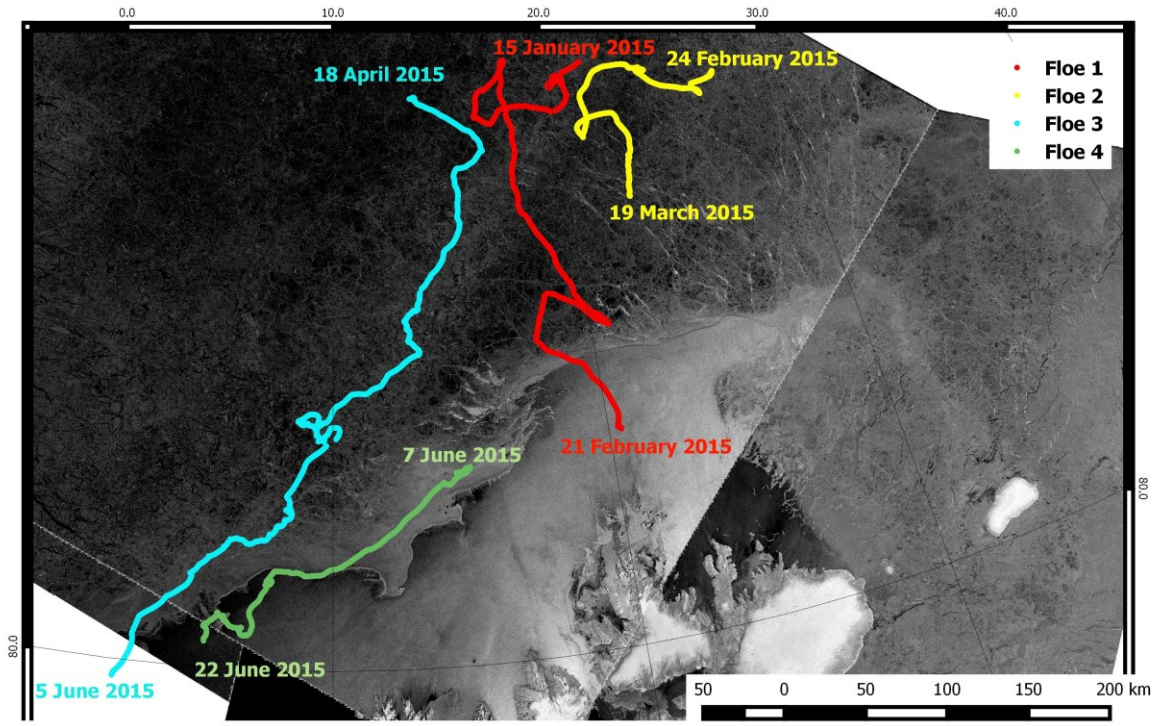

RADARSAT images: 21 & 22 January 2015
RADARSAT-2 images provided by NSC/KSAT under the Norwegian-Canadian RADARSAT agreement 2013
(C) MacDonald, Dettwiler and Associates
Map created by Norwegian Polar Institute / Jennifer King

Map showing drift trajectories for all 4 ice-floes with start and end points. The continent below is the Svalbard archipelago. (Created by Jennifer King, the Norwegian Polar Institute)